Geothermics 111 (2023) 102702

Contents lists available at ScienceDirect

Geothermics

journal homepage: www.elsevier.com/locate/geothermics

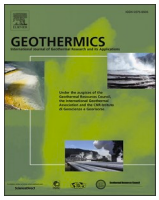

The subsurface thermal state of Svalbard and implications for geothermal potential

Kim Senger [a,*], Matthijs Nuus [a,b,c], Niels Balling [d], Peter Betlem [a,e], Tom Birchall [a], Hanne H. Christiansen [f], Harald Elvebakk [g], Sven Fuchs [h], Malte Jochmann [a,i], Peter Klitzke [j], Kirsti Midttømme [k], Snorre Olaussen [a], Christophe Pascal [l], Nil Rodes [a], Aleksey Shestov [m], Aleksandra Smyrak-Sikora [a], Peter James Thomas [k]

[a] Department of Arctic Geology, The University Centre in Svalbard, PO Box 156, 9171, Longyearbyen, Norway
[b] School of Engineering and Natural Sciences, University of Iceland, Sæmundargata 2, 102, Reykjavík, Iceland
[c] Department of Earth Sciences, Utrecht University, Heidelberglaan 8, 3584, CS Utrecht, The Netherlands
[d] Department of Geoscience, Aarhus University, Høegh-Guldbergs Gade 2, 8000 Aarhus C, Denmark
[e] Department of Geosciences, University of Oslo, Sem Sælands vei 1, 0371 Oslo, Norway
[f] Department of Arctic Geophysics, The University Centre in Svalbard, UNIS, P.O. Box 156, 9171 Longyearbyen, Norway
[g] Geological Survey of Norway (NGU), Leiv Eirikssons vei 39, 7040 Trondheim, Norway
[h] Helmholtz Centre Potsdam, GFZ German Research Centre for Geosciences, Section Geoenergy, Potsdam, Germany
[i] Store Norske Energi AS, Postboks 613, 9171 Longyearbyen, Norway
[j] Federal Institute for Geosciences and Natural Resources (BGR), Hannover, Germany
[k] NORCE, Norwegian Research Centre, Postboks 22, Nygårdstangen 5838 Bergen, Norway
[l] Institute of Geology, Mineralogy and Geophysics, Ruhr University Bochum, Germany
[m] Department of Arctic Technology, The University Centre in Svalbard, UNIS, P.O. Box 156, 9171 Longyearbyen, Norway

ARTICLE INFO

Keywords:
Geothermal potential
Sustainable energy
Arctic
Svalbard
Heat flow

ABSTRACT

Svalbard is a High Arctic Archipelago at 74–81°N and 15–35 °E under the sovereignty of Norway. All settlements in Svalbard, including the capital of Longyearbyen (population 2400), currently have isolated energy systems with coal or diesel as the main energy source. Geothermal energy is considered as a possible alternative for electricity production, as a heat source in district heating systems or harnessed for heating and cooling using geothermal heat pump installations. In this contribution we present the until now fragmented data sets relevant to characterize and assess the geothermal potential of Svalbard. Data sets include petroleum and deep research boreholes drilled onshore Svalbard, 14 of which have recorded subsurface temperature data at depths below 200 m. Geothermal gradients on Spitsbergen vary from 24 °C/km in the west to 55 °C/km in the south-east, with an average of 33 °C/km. Four deep research boreholes were fully cored and analyzed for thermal conductivity. These analyses were complemented by thermal conductivity calculated from wireline logs in selected boreholes and four measurements on outcrop samples. 1D heat flow modelling on five boreholes calibrated with the measured thermal conductivities offers insights into heat transfer through the heterogeneous sedimentary succession. Offshore petroleum boreholes in the south-western Barents Sea and marine heat flow stations around Svalbard provide a regional framework for discussing spatial variation in heat flow onshore Svalbard, with emphasis on the effects of erosion and deposition on the thermal regime. We conclude that Svalbard's geology is well suited for geothermal exploration and potential production, though challenges related to permafrost, the presence of natural gas, heterogeneous reservoir quality and strongly lateral varying heat flow need to be adequately addressed prior to geothermal energy production. Specifically for Longyearbyen, high geothermal gradients of 40–43 °C/km in the nearest borehole (DH4) suggest promising sub-surface thermal conditions for further exploration of deep geothermal potential near the settlement.

* Corresponding author.
E-mail address: kims@unis.no (K. Senger).

https://doi.org/10.1016/j.geothermics.2023.102702
Received 6 December 2022; Received in revised form 27 February 2023; Accepted 9 March 2023
Available online 2 April 2023

1. Introduction

Geothermal energy is a renewable energy source that experiences revitalized interest considering the ongoing energy transition from a fossil-fuel dominated energy towards renewable energy sources (e.g., Lund and Toth, 2021; Moya et al., 2018; Smith, 2019). The need for new energy sources has been further exacerbated by the recent geopolitical developments. Onshore mainland Norway, geothermal energy is thus far investigated on a relatively small scale and present-day limited to shallow-medium depth geothermal systems contributing to district and individual heating (e.g., Pascal, 2022) utilizing heat pumps to extract heat from 100 to 500 m deep boreholes (Midttømme et al., 2020). On the Norwegian Arctic archipelago of Svalbard, geothermal gradients are higher than in mainland Norway and medium-deep geothermal systems are seen as a potential alternative to Longyearbyen's coal-fuelled power plant for both heating and electricity (Midttømme et al., 2015b). The present plans focus on risk-mitigation by extracting heat from a depth of 1.5–2 km using a deep borehole heat exchanger (DBHE; SNSK, 2022). Deeper boreholes targeting potential aquifers, developing enhanced geothermal systems or DBHE at depths > 5 km and temperatures exceeding 150 °C could generate electricity (Schintgen, 2015), but imply high investment costs and risks. A DBHE system lowers the risk by removing the need for fluid injection, circulation and production in the reservoir. Significant experience was gained from DBHE utilization in abandoned petroleum wells in Switzerland (Kohl et al., 2002). DBHE systems are, through their closed-loop nature, less dependant on the geological subsurface parameters but require site-specific design optimization for optimum production (Alimonti et al., 2021).

Understanding the present-day thermal state of Svalbard is critical to make data-driven estimates of the archipelago's geothermal potential. Exploration borehole data from onshore Svalbard suggest high spatial variability, with geothermal gradients ranging from 24 °C/km to 55 °C/

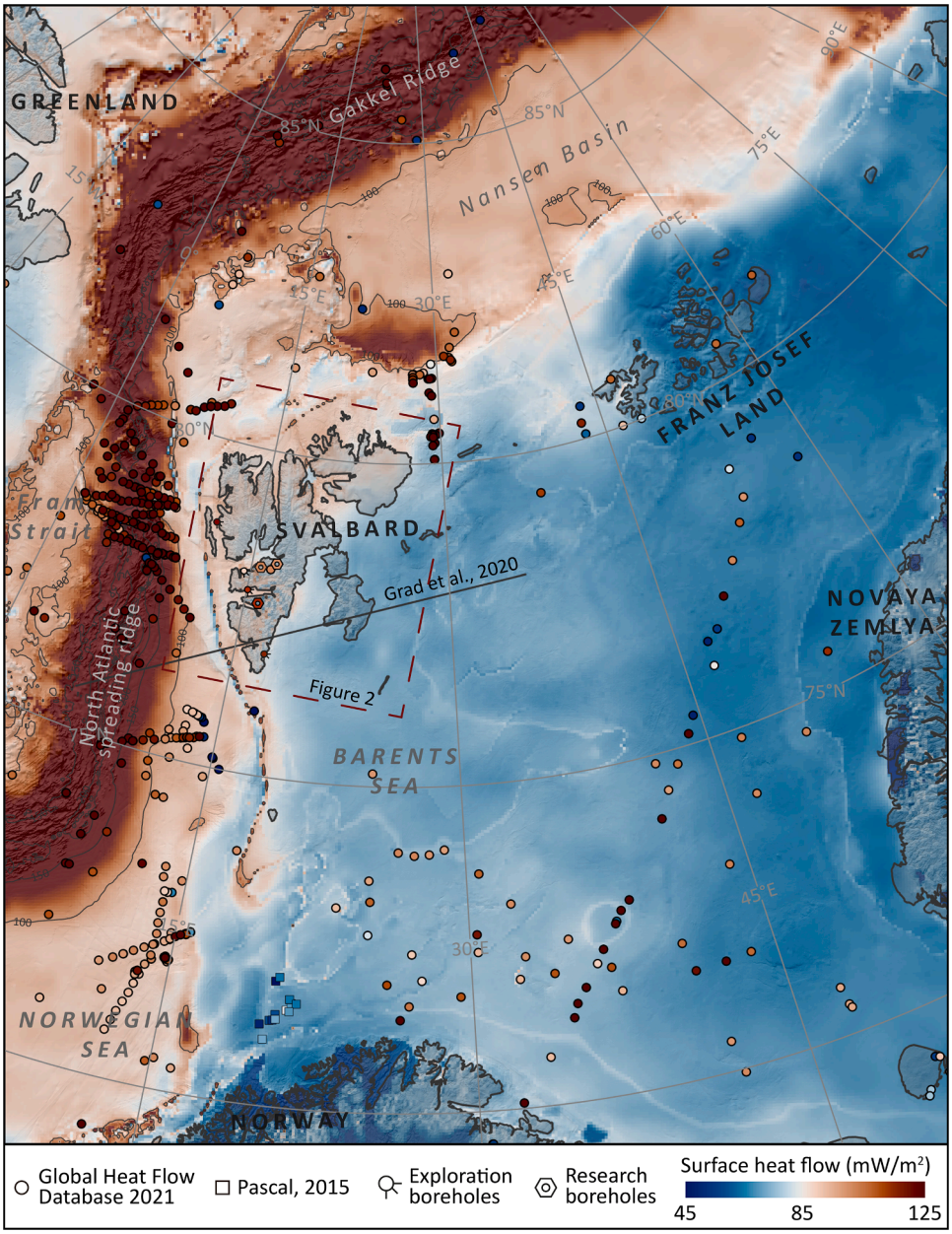

Fig. 1. Regional geodynamic setting of the Svalbard archipelago, illustrating the major plate boundaries and key tectonic elements. The base map illustrates regional heat flow from the thermal model of Klitzke et al. (2016). Point data show heat flow estimates from petroleum exploration boreholes or offshore heat flow stations, as provided in the global heat flow database (Fuchs et al., 2021).

km (Betlem et al., 2019; Olaussen et al., 2023). However, understanding how and why the thermal regime varies spatially and temporally (both seasonally and through geological time) is of utmost importance also for improving models of glacier evolution (e.g., Schäfer et al., 2014), estimating permafrost thickness (e.g., Etzelmüller et al., 2011; Humlum, 2005), mapping the gas hydrate stability zone (e.g., Betlem et al., 2021, 2019), characterizing petroleum systems (e.g., Olaussen et al., 2023), deciphering subsurface fluid flow through Arctic groundwater systems (e.g., Haldorsen and Heim, 1999) and in general understanding the thermal and geological evolution of the area (e.g., Sundvor and Austegard, 1990).

Decision makers in the geothermal industry require quantitative resource assessments to identify economically suitable projects. In the past, surface thermal flux was the first quantitative method for estimating geothermal potential, while the United States Geological Survey's systematic volumetric method was used in regional assessments (Ciriaco et al., 2020 and references therein). Both of these can be applied in regional screening, but other methods such as the lumped-parameter and decline curve methods are only applicable once geothermal fields start producing (Axelsson et al., 2005; Ciriaco et al., 2020 and references therein). Numerous studies quantify the geothermal potential of various regions with varying data coverage and geological setting, including Oklahoma (Harrison et al., 1982), Egypt (Swanberg et al., 1983), Korea (Lee et al., 2010), Canada (Jessop et al., 1991) Denmark (Mathiesen et al., 2022; Nielsen et al., 2004) and Norway (Pascal et al., 2010b). For Svalbard, the geothermal assessment of the data-sparse Canadian Anticosti Island by Gascuel et al. (2020) is arguably most relevant.

The High Arctic (i.e. 75–90 °N) remains one of the least explored parts of the world, largely due to its inaccessibility and extremely high logistical costs. Nonetheless, offshore heat flow density (referred to as 'heat flow' herein) has been measured in the Arctic Basin since the 1960s (Lachenbruch and Marshall, 1969). Closer to our study site, marine heat flow measurements focused on the transform margin west of Svalbard (Fig. 1; Crane et al., 1991, 1988; Vogt and Sundvor, 1996). Most of the work was motivated to test models of oceanic spreading and rifting. Heat flow along the west Svalbard margin was also derived from

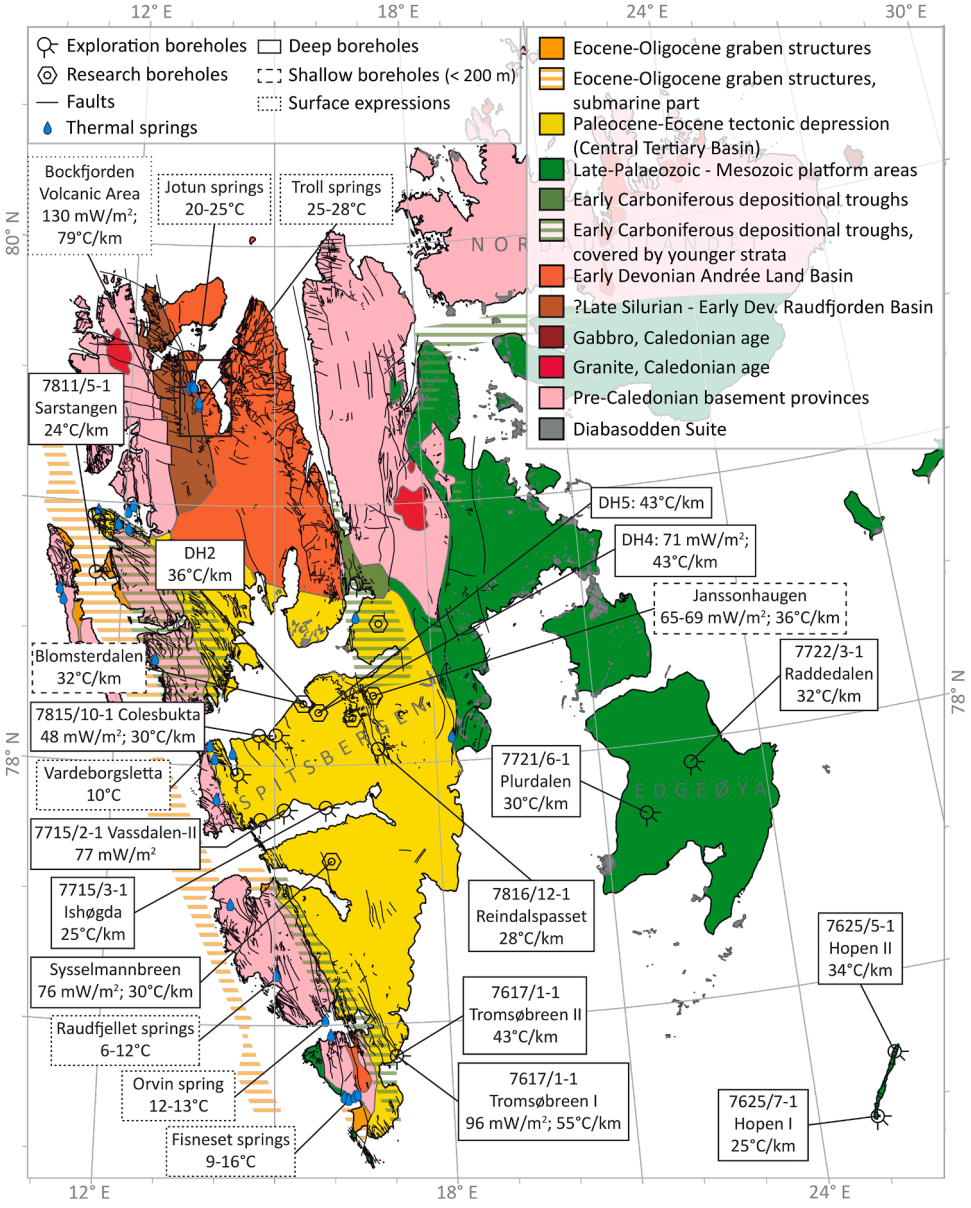

Fig. 2. Structural element map of Svalbard, modified from Dallmann (2015), highlighting the major tectonic elements, faults, thermal springs and boreholes. Boreholes with temperature data are highlighted with geothermal gradients and calculated heat flow values where available. Further details on the heat flow calculation methods and the reference are provided in Electronic Supplementary Material Table 1.

bottom-simulating reflections (BSRs) related to the gas hydrate province at Vestnesa (Vanneste et al., 2005). Khutorskoy and Akhmedzianov (2008) and Khutorskoi et al. (2009) compiled marine heat flow data around Svalbard and Franz Josef Land, while Klitzke et al. (2016) presented a regional Barents-Kara Sea lithosphere-scale thermal model. Grad and Majorowicz (2020) present 2D heat flow models across the Hornsund-Storfjorden fjords, which is revisited in the discussion.

Colgan et al. (2022) discuss marine and terrestrial heat flow data from Greenland, including the Fram Strait data west from Svalbard. The data are compiled in a single database (Colgan and Wansing, 2021). Petroleum exploration in the Canadian Sverdrup Basin resulted in several geothermal-focussed studies utilizing deep exploration borehole data (Chen et al., 2018; Jones et al., 1990, 1989; Majorowicz and Embry, 1998).

The Geological Survey of Norway (NGU)'s HeatBar project investigated the heat flow on the Norwegian Barents Sea and northern Norway (Pascal et al., 2010a). HeatBar also provided thermal conductivity analyses of two research boreholes onshore Svalbard (Sysselmannbreen and DH1; Pascal et al., 2010a). The Barents Sea data, including marine heat flow data near Svalbard, were summarized by Pascal (2015).

Onshore Svalbard, the geothermal potential is also illustrated by numerous geothermal springs, many of which were known for decades (Fig. 2; Banks et al., 1997; Jamtveit et al., 2006; Lauritzen and Bottrell, 1994; Olichwer and Tarka, 2018; Reigstad et al., 2011; Salvigsen and Elgersma, 1985). Year-round outflow temperatures range from a few degrees above freezing at the western and southern springs to as much as 30 °C at the springs in the vicinity of the Quaternary Bockfjorden Volcanic Complex in northern Spitsbergen (Fig. 2). Here, local heat flows and geothermal gradients are calculated to reach 130 mW m^{-2} (Vagnes and Amundsen, 1993) and 79 °C/km, respectively (Amundsen et al., 1987).

Svalbard's deep geothermal resource potential was first addressed in the early 2010s by a joint project between Christian Mikkelsen Research (CMR, now part of NORCE), Norwegian Seismic Array (NORSAR) and the local coal mining company Store Norske Spitsbergen Kulkompani (SNSK; Midttømme et al., 2015b). Svalbard was subsequently included in regular country updates for Norway (Midttømme et al., 2015a). This milestone project laid the foundation for further work by gaining access to the fragmented temperature data from petroleum exploration boreholes, conducting initial heat flow modelling on a few boreholes and testing fibre optic thermistors in the Longyearbyen CO_2 lab research boreholes and several coal exploration boreholes. The project concluded that Longyearbyen is the settlement in Svalbard with the best geothermal data coverage and highest geothermal gradient. Risk-mitigation measures, such as seismic and non-seismic data acquisition, exploration drilling or the use of a DBHE are necessary to proceed with deep geothermal projects.

In parallel, temperature data from 18 petroleum exploration boreholes drilled onshore Svalbard from 1961 to 1994 (Senger et al., 2019), were compiled by Betlem et al. (2018). Selected petroleum boreholes were subjected to 1D heat flow modelling as part of a University of Utrecht/University Centre in Svalbard (UNIS) thesis (Nuus, 2020). The same data also served as input for onshore gas hydrate stability zone modelling by Betlem et al. (2019) and were put in a petroleum systems context by Olaussen et al. (2023).

Beka (2016) concentrated on the regional mapping of geothermal potential using magnetotelluric (MT) data. The MT method maps subsurface resistivity and is routinely used in geothermal exploration (e.g., Hacıoğlu et al., 2021; Ledo et al., 2021). In Svalbard, MT profiles were acquired in the major and accessible valleys of Nordenskiöld Land (Beka et al., 2015, 2016) and on Brøggerhalvøya in western Spitsbergen (Beka et al., 2017a). The last profile was acquired near the research settlement of Ny Ålesund where the shallow geothermal potential was addressed by Iversen (2013).

Ringkjøb et al. (2020) conducted a modelling study of a wide range of electricity sources considering the energy transition in Longyearbyen, but unfortunately did not include deep geothermal potential due to the high uncertainty in both the resource potential and costs. Most recently, SNSK led a feasibility project to use geothermal energy to provide heat to a new building, the "Folkehøgskole" campus, in Longyearbyen, using a DBHE-system with industrial heat pumps (Richter, 2021; SNSK, 2022). The project was carried out in cooperation with the Norwegian geothermal company Geothermal Energy Nordic (GTML) and UNIS. The main conclusions of the project were that geothermal potential exists but is economically more interesting if conducted for more than just the one building due to the high mobilization and drilling costs of a petroleum drilling rig. In addition, the local challenges of drilling and producing heat through permafrost would require drilling directly on bedrock and other site-specific adaptations.

Furthermore, as Longyearbyen intends to replace fossil fuels (locally produced coal and imported diesel) with renewable energy sources, seasonal heat storage (i.e. geothermos) in the subsurface is being considered (Ylvisåker, 2021). One 200 m deep borehole was drilled in 2020 near Longyearbyen's airport to study the thermal properties of the shallow subsurface and model the capacity for seasonal heat storage (Kurttila, 2021; Snoen, 2021).

Nonetheless, several critical knowledge gaps remain to quantify the geothermal resource potential of Svalbard and reduce the uncertainties. Firstly, all available temperature from relevant boreholes (petroleum and coal exploration and deep and shallow research boreholes) must be synthesized to identify spatial variability in the heat flow regime. These data need to be put in a geological context. Secondly, a synthesis of measured relevant parameters (thermal conductivity, density, heat capacity etc.) within Svalbard's heterogeneous geology is needed to constrain 1D-2D-3D thermal models.

In this contribution we address these knowledge gaps through the following objectives: 1) synthesize subsurface temperature data from onshore Svalbard and its immediate surroundings, 2) systematically present new thermal conductivity data from drill cores, 3) generate data-driven 1D heat flow models at selected borehole sites, 4) integrate thermal data with the regional and local geological context to both decipher geological evolution but also to identify concrete drilling targets and 5) identify knowledge gaps that must be addressed before Svalbard's deep geothermal potential can be fully utilized.

2. Geological setting and thermal evolution

The Svalbard archipelago, Norway, comprises all islands between 74 and 81 °N and 15–35 °E and is geologically situated in the north-western corner of the Eurasian continental plate. The archipelago is bounded by passive margins to the west (i.e. North Atlantic) and north (i.e. Eurasia Basin). The North Atlantic spreading ridge is located 100 km from the western coast of Spitsbergen (Fig. 1), while the ultra-slow spreading axis along the Gakkel Ridge is 500 km from the northern coast of Svalbard (Faleide et al., 2008; Gac et al., 2020). Regional heat flow maps show increased heat flow from the south-east to the north and west (Fig. 1; Antonovskaya et al., 2018; Dumais et al., 2022; Khutorskoi et al., 2022; Klitzke et al., 2016; M.D. et al., 2015; Slagstad et al., 2009).

Svalbard is the exposed part of the subsurface of the Barents Shelf. The outcropping, nearly complete sedimentary succession from Ediacaran to Holocene is punctuated by two major hiatuses affecting the Upper Cretaceous and most of the late Paleogene and Neogene strata (Fig. 3; Dallmann, 2015). Three crystalline basement provinces are recognized; the southwestern and northwestern provinces in Spitsbergen and the northeastern basement province in Spitsbergen and Nordaustlandet. The northeastern basement province was intruded by Caledonian granites and gabbro (Dallmann, 2015).

The main post-Caledonian tectonic evolution in Svalbard (Fig. 3) can be divided into four main events: 1) faulting along N-S trending long-lived tectonic lineaments, e.g., Billefjorden and Lomfjorden Fault zones with associated Upper Paleozoic extensional basins; 2) Mesozoic subsiding basin with Early Cretaceous magmatism; 3) Cenozoic

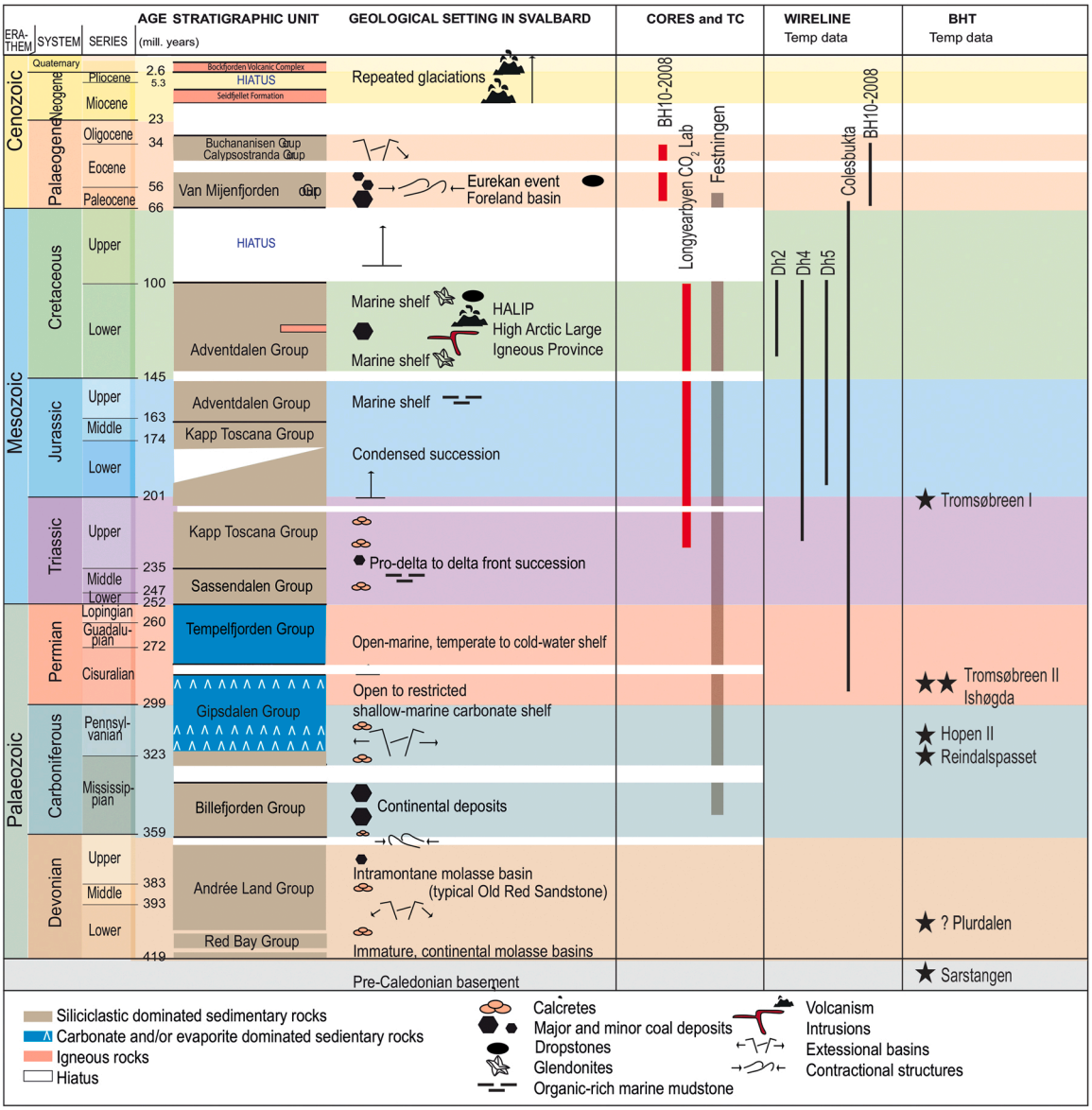

Fig. 3. Stratigraphic column with main tectono-thermal events and relevant data coverage (thermal conductivity on drill cores, wireline temperature logs and bottom hole temperatures, BHT). Figure modified from Smyrak-Sikora et al. (2022). Details on the temperature measurements available are provided in Electronic Supplementary Material Table 2.

contraction; i.e. the West Spitsbergen Fold-and-Thrust Belt (WSFTB) and 4) late Neogene uplift and glaciation. The two last tectonic events are the most influential with respect to the current geothermal gradient and the paleotemperature gradient of the Cenozoic cf., Marshall et al. (2015).

Emplacement of large igneous provinces and local magmatism also affect the geothermal gradient. The Early Cretaceous High Arctic Large Igneous Province (HALIP) is manifested by igneous intrusions emplaced in the Upper Paleozoic to Lower Cretaceous sediments commonly seen as sills with less common dykes and extrusive basalts only reported in Kong Karls Land (Senger and Galland, 2022; Senger et al., 2014). The HALIP in Svalbard is dated to 124.5 Ma (i.e. Barremian) with U-Pb dating (Corfu et al., 2013). Swarms of HALIP sills have affected maturation of Middle Triassic organic rich marine mudstones in larger areas in Svalbard (Brekke et al., 2014; Hubred, 2006).

In addition, localized magmatism occurred in both the Miocene and Quaternary. The Miocene event is manifested by plateau lava flows of the Seidfjellet Formation highlighting the paleo-topography developed within the Devonian succession in NW Spitsbergen (Dallmann, 2015; Prestvik, 1978). These lavas were presumably emplaced by fissure eruption along regional fault zones parallel to the N-S trending transtensional lineament of the western margin of Spitsbergen and its commonly linked to the opening of the North Atlantic sea floor spreading. Recent volcanism is also reported from the offshore areas south (Mørk and Duncan, 1993) and north (Geissler et al., 2019) of Svalbard. Quaternary magmatism is represented by the Bockfjorden Volcanic Complex with three volcanic centers located along the Breibogen Fault Zone in NW Spitsbergen (Fig. 2; Amundsen et al., 1987; Dallmann et al., 1999; Skjelkvåle et al., 1989). This volcanism has geochemical affinity to the Gakkel Ridge located northwards (Griffin et al., 2012).

Following the Caledonian orogeny and subsequent mountain chain collapse, thick Devonian continental deposits (i.e. Old Red Sandstone; Fig. 3) were deposited in fault-bounded basins. These sandstone-dominated deposits are well exposed in northern Spitsbergen but due to the regional southerly dip also underlie the main settlements of Longyearbyen and Barentsburg at sufficient depths to represent possible geothermal targets. The Late Devonian Ellesmerian (locally called Svalbardian) compressional event deformed some of these sediments.

The regionally deposited Early Carboniferous Billefjorden Group comprises fluvial deposits with some coal seams (Gjelberg and Steel, 1981), deposited in a tropical and humid floodplain environment in interior continental basins. In the transitions between Mississippian and Pennsylvanian carbonate siliciclastic syn-rift deposits were deposited in half-grabens along the N-S trending fault zones, such as the Lomfjorden and Billefjorden fault zones (Smyrak-Sikora et al., 2019, 2021). In the mid-Pennsylvanian a major carbonate platform was established across Svalbard and the greater Barents Sea. In central and western Spitsbergen a renewed extensional tectonic phase occurred in the Mid-Permian. Continuing northward drift of Svalbard and the closure of the Uralian Seaway led to a shift from warm-water to cold-water carbonates (Stemmerik, 2008).

The Triassic marks a shift from carbonate-dominated to siliciclastic-dominated deposition. A major north-westward prograding delta system crossed the entire Barents Shelf during this period, resulting in the deposition of shallow-marine to deep shelf sandstones and organic-rich shales (Anell et al., 2014).

Siliciclastic deposition continued in the Jurassic, when a condensed sandstone-dominated succession forms the major reservoir intervals in the Barents Shelf and the local CO_2 storage reservoir near Longyearbyen (Braathen et al., 2012; Olaussen et al., 2019). The caprock comprises regional shale-dominated successions with Upper Jurassic to Lower Cretaceous organic rich marine mudstone units (Koevoets et al., 2018).

The Upper Jurassic to Lower Cretaceous marked a shift in the depositional patterns, related to uplift in the north and resulting in southward-propagating sedimentary wedge comprising both marine and terrestrial sandstones and shales. The Helvetiafjellet Formation was deposited at the same time as the major HALIP magmatic pulse and coincides with HALIP-related lava flows and volcanic activity in the eastern islands of Kong Karls Land.

Paleogene compression resulted from Svalbard's movement past northern Greenland, forming the West Spitsbergen Fold-and-Thrust-Belt and its associated foreland basin called Central Spitsbergen Basin (CSB). Continental and marine siliciclastic deposits filled the basin (Helland-Hansen and Grundvåg, 2021). The coal-bearing strata forming the foundation for economic activity in Svalbard over the past century were deposited at the base of the CSB.

In summary, Svalbard offers a lithologically diverse succession with distinct thermal properties.

3. Data and methods

We integrate all available data, as listed in Table 1, to quantify the thermal state of Svalbard.

3.1. Borehole data

We have integrated all available and relevant data from onshore petroleum, coal and research wells, summarized in Supplementary Material Table 1.

3.1.1. Bedrock research boreholes

Fully-cored research boreholes are summarized in Senger et al. (2019) and include two boreholes across the Permian-Triassic boundary in Deltadalen (with no thermal conductivity or temperature measurements; Zuchuat et al., 2020), eight boreholes with Mesozoic stratigraphy in Adventdalen and one borehole through the Cenozoic at Sysselmannbreen.

Eight boreholes, DH1-DH8, were drilled and fully cored near Longyearbyen from 2007 to 2013 as part of a CO_2 sequestration feasibility project (Braathen et al., 2012; Olaussen et al., 2019 and references therein). Cumulatively the drill cores comprise 4.5 km of stratigraphy. The deepest borehole DH4 is 972 m deep and covers Early Cretaceous to Late Triassic strata. Thermal conductivity was measured on the drill cores (Electronic Supplementary Material Table 7). In addition, wireline logging was conducted in selected intervals in four boreholes (DH1, DH2, DH4 and DH5) where also temperatures were measured (Elvebakk, 2008, 2010). In the upper part of DH2 (0–440 m) temperatures were measured twice. In 2007 standard wireline logging was applied (Elvebakk, 2008) while in 2014 fibre optic temperature sensing was conducted.

The BH10–2008 borehole (often referred to as "Sysselmannbreen" for its location) was drilled by SNSK in 2008 as part of a research project to study clinoform successions (Johannessen et al., 2011). The 1085 m deep borehole is the deepest fully cored borehole in Svalbard and covers the Late Paleocene to Eocene succession. Drill cores were used for thermal conductivity and wireline logging including temperature were conducted (Elvebakk et al., 2008; Pascal et al., 2010a). In addition, temperature monitoring was initiated but experienced technical issues with the equipment.

3.1.2. Petroleum exploration wells onshore svalbard

18 petroleum exploration wells were drilled onshore Svalbard from

Table 1
Overview of data sets used to characterize the ground thermal state of Svalbard. NPD = Norwegian Petroleum Directorate. Details on all data sets are included in Electronic Supplementary Material Tables 2, 3 and 4.

Data set	Applications	Source
Onshore boreholes		
Onshore petroleum exploration wells (n = 18, 10 with temp. data)	Subsurface temperature Rock properties	This study, Betlem et al. (2018), Senger et al. (2019)
Onshore research wells (n = 11, 4 with temp. data)	Thermal conductivity Subsurface temperature Rock properties	This study, Olaussen et al. (2019), Elvebakk et al. (2008), Pascal et al. (2011)
Onshore coal exploration wells	Subsurface temperature	This study, Christiansen (2009)
Shallow (down to 100 m) boreholes for permafrost monitoring across mainly western Svalbard (n = 18, all with temperature data)	Permafrost temperature observations	Isaksen et al. (2000) Christiansen et al. (2010), Christiansen et al. (2021)
One shallow borehole to 200 m, geothermos project	Subsurface temperature Thermal conductivity	Snoen (2021), Kurttila (2021)
Rock samples from outcrops (n = 4)	Thermal conductivity	Daleng and Aftret (2021)
Offshore boreholes		
Offshore exploration wells	Subsurface temperature	This study, Pascal (2015), NPD
Offshore heat flow stations	Spatial thermal gradient variation	Khutorskoi et al. (2009)
Numerical modelling		
Thermal conductivity predictions from wireline logs	Thermal conductivity	This study, Fuchs et al. (2015)
Heat flow modelling	Heat flow	This study, Pascal et al. (2010a)
Onshore permafrost thickness modelling	Gas hydrate stability zone modelling	Betlem et al. (2019)
Key publications		
Thermal springs	Surface heat flow values Spring water temperatures	Banks et al. (1997), Jamtveit et al. (2006), Lauritzen and Bottrell (1994), Olichwer and Tarka (2018), Reigstad et al. (2011), Salvigsen and Elgersma (1985)
Magnetotelluric and TEM data	Lateral extent of conductors Crustal conductivity structure	Beka et al. (2016), Beka et al. (2017a), Beka et al. (2017b), Selway et al. (2020)

Table 2
Overview of exploration and relevant research boreholes in Svalbard and available temperature data. Refer to Electronic Supplementary Material Table 3 for details on the boreholes and data availability. TD = total depth. Further details on the boreholes, including alternative well names and Norwegian Petroleum Directorate's well identifiers are provided in Senger et al. (2019).

Well	Total depth	Geothermal gradient Top - TD 500 m - TD	T at 1000 m Modelled Modelled Measured	K Average Range	Q
	m	° C/km	°C	W/m/K	mW m^{-2}
Sysselmannbreen > 500 m depth 1000 m measured	1085	31.46 ± 0.02 34.75 ± 0.02	29.16 ± 0.02 29.96 ± 0.01 29.15	2.86 1.75 - 6.2	76
DH2 > 250 m depth 1000 m measured	856.3	29.77 ± 0.02 36.43 ± 0.01	28.27 ± 0.03 32.69 ± 0.01 No data	3.35 1.3 - 6.5	x
DH4 > 500 m depth 972 m measured	969.7	42.73± 0.07 39.97 ± 0.04	37.0 ± 0.16 36.35 ± 0.04 31.61	2.55 1.84 - 5.1	71
DH4 (start depth = 240 m)	241.6 - 899.4	46.14 +- 0.03	38.17 ± 0.06	See above	X
DH5 >500 m depth 1000 m measured	702	43.92 ± 0.02 42.89 ± 0.02	38.89 ± 0.05 38.93 ± 0.03 No data	No data	X
Colesbukta > 500 m depth 1000 m measured	3173	29.95 ± 0.10 30.76 ± 0.10	29.73 ± 0.18 28.75 ± 0.21 27.09	No data	48
Ishøgda 1000 m measured	3304	27.1	27.3 ± 0.2 No data	No data	x
Reindalspasset 1000 m measured	2315	31.4 ± 2.5	31 ± 11 No data	No data	x
Sarstangen 1090 m measured	1113	23.9	23.9 26.0	No data	x
Tromsøbreen 993 m measured	993	43.83 ± 0.78	56.32 ± 1.3 56.0	No data	96
Tromsøbreen II 1000 m measured	2337	43.3 ± 0.3	43.6 ± 7.7 No data	No data	x
Hopen I 1000 m measured	908	27.76 ± 0.45 33.39 ± 0.27	32.87 ± 0.31 32.70 ± 0.15 No data	No data	x
Hopen 2 1000 m measured	2840	25.39 ± 1.37	30.43 ± 2.69 No data	No data	x
Raddedalen 1000 m measured	2823	31.9	31.9 No data	No data	x
Plurdalen 1000 m measured	2351	23.6 ± 1.5	33.8 ± 1.8 No data	No data	x
Plurdalen forced through near 0 (added 4 points at 0,0)	x	28.7 ± 1.9	30.9 ± 3.1	No data	x
B2, Blomsterdalen	198	32		3.47	
Average geothermal gradients					
All wells – all depths		36.77			
All wells except Tromsøbreen I and II – all depths		32.80			
All wells – depths > 500 m		37.09			
All wells except Tromsøbreen I and II – depths > 500 m		32.32			

1961 to 1994 and offer variable types of data useful for estimates of geothermal potential of Svalbard (Electronic Supplementary Material Table 1; Senger et al., 2019). The deepest borehole, Ishøgda, was drilled in 1965–66 by Caltex and penetrates 3304 m of Paleocene to Lower Permian strata. Ten of the petroleum exploration wells offer temperature data (Fig. 2, Electronic Supplementary Material Tables 3 and 4). Three of these are single bottom hole temperatures (BHT; Fig. 3). The Colesbukta (referred to as "Grumantskaya" in Soviet/Russian literature and 7815/10-1 with NPD's nomenclature; Senger et al., 2019) borehole offers the most detailed temperature log. 12 wells offer wireline logs of variable coverage and quality (Electronic Supplementary Material Table 1). Data is unfortunately fragmented and incomplete, with many drill cores lost. The Svalbard Rock Vault project has systematically gathered and digitized information from numerous sources including the archives of Norsk Polar Navigasjon, BarentzGruppen and the Tromsøbreen II archive in Lund, with an overview provided by Senger et al. (2022).

3.1.3. Coal exploration boreholes

More than 400 coal exploration boreholes were drilled by SNSK between the 1940s and 2014 to depths of up to 700 m, focusing mainly on exploring for Cenozoic coal within the CSB. Temperature was measured in several of those, but the data mainly show the temperature of the drilling fluid following drilling and are therefore rarely usable to quantify the geothermal gradient. Several of the more recent boreholes, for instance BH13A at Ispallen, were equipped with thermistors or fiberoptic cables and yielded useful temperature data. Several boreholes, amongst them a 90 m deep borehole (LF-B-1 Lunckefjell) drilled at an altitude of more than 1000 masl, contributed to temperature data in the Global Terrestrial Network for Permafrost Database (Christiansen, 2009).

3.1.4. Cryosphere research boreholes

Shallow (i.e. < 100 m depth) boreholes are routinely drilled onshore Svalbard in both periglacial (Isaksen et al., 2000) and glacial (Motoyama et al., 2008) environments to characterize the geothermal heat flow, but primarily for ground thermal monitoring. These are of importance to infer the base of the permafrost, to observe permafrost thermal changes due to the ongoing climatic changes and to calibrate models of thermal fluxes near glaciers. At Janssonhaugen, 16 km east-south-east of Longyearbyen (Fig. 2), heat flow is estimated to be 69 ± 2 mW m^{-2} (Isaksen et al., 2001). Other boreholes with temperature measurements include the 200 m borehole drilled in March 2020 to test subsurface energy storage near Hotellneset (Electronic Supplementary Material Table 1; Kurttila, 2021; Snoen, 2021).

For permafrost monitoring as part of the Svalbard Integrated Observing System (SIOS) infrastructure five main sites at Longyearbyen, Barentsburg, Hornsund, Kapp Linne and Ny-Ålesund each have several typically around 10–50 m deep boreholes with continuous ground thermal observations (Christiansen et al., 2021). During the International Polar Year (IPY; Christiansen et al., 2010) in 2007–2008 12

boreholes were drilled in central and western Svalbard typically down to 10 m for permafrost observations. As part of the ongoing SIOS InfraNOR project several of the existing IPY shallow boreholes around in the Adventdalen and Longyearbyen area have been extended to 20 m depth, with one 100 m borehole drilled and instrumented in Endalen. All SIOS permafrost observation boreholes have continuous ground temperature monitoring for studying the effects of climate change on the ground thermal regime in the top of the permafrost. The ground ice content and drilling methods of the SIOS permafrost boreholes have been mapped (Christiansen et al., 2021).

Drilling and temperature measurements down to 118–289 m depth on 3 boreholes the Nordaustlandet ice cap suggests heat flow of 40 mW m^{-2} (Motoyama et al., 2008; Zagorodnov et al., 1989), still affected by Weichselian glaciations (Schäfer et al., 2014). A 120 m deep ice core was also recovered from Lomonosovfonna in eastern Spitsbergen in 1997. The measured temperatures indicate a low geothermal gradient of 0.011 ± 0.004 °C m^{-1} (i.e. 11 °C/km) in the bottommost 20 m, with the ice likely damping the geothermal heat flow (van de Wal et al., 2002).

Clearly, the geothermal heat flow will also influence both glacial and periglacial environments from beneath. However, the large spatial and depth variability in temperatures recorded in glacial and permafrost areas suggests that temperatures from deep boreholes beneath the permafrost are most reliable to estimate the geothermal heat flow.

3.1.5. Physical drill core data

Supplementary Material Table 5 synthesizes the analyses conducted on Svalbard's drill cores.

3.2. Thermal conductivity

3.2.1. Sysselmannbreen and Dh1/Dh2 boreholes

Thermal properties were measured on core samples from the Sysselmannbreen and DH1 boreholes in the framework of the HeatBar project (Pascal et al., 2010a). The samples of shales and siltstones were measured at Aarhus University (AU), whereas sandstones and conglomerates were measured at the Geological Survey of Norway (NGU).

NGU employed an in-house transient method based on Middleton (1993). Firstly, the samples were cut in 20 mm high and 35 mm wide disks and water-saturated. Constant heat flow was then applied to the top of each measured rock sample, using a radiative heat source with constant temperature of 300 ± 2 °C located 1 cm above the sample. Insulation was prescribed to the remaining sample surfaces and temperatures were measured at its base. Finally, thermal diffusivity was derived from the measured temperature-time plot and thermal conductivity calculated from thermal diffusivity, density (measured using Archimedes principle), and an assumed value for specific heat capacity (i.e. 850 J/(kg K) in the present case). Quality control was carried out by measurements on the standard material Pyroceram 9606. The apparatus at NGU was improved in December 2005 and the error of the thermal diffusivity measurements was within ± 5% at the time of the measurements reported hereafter (i.e. June 2009). Further details about the method can be found in Kalskin Ramstad et al. (2008).

The sampled shales and siltstones were too weak to be prepared for measurements at NGU and were analyzed at AU using the less aggressive needle probe method. This method is a reliable and widely used method to determine thermal conductivity of different materials including geomaterials. It is a cylindrical source method with its theoretical framework outlined in Blackwell (1954) and applied in terms of 'small needle probes' by Von Herzen and Maxwell (1959) to measure thermal conductivity of deep-sea sediments. The needle probes used by AU were of a similar type. The probe consists of a metal tube of surface-coated brass containing a heating wire of manganin and insulating ceramic tubes with holes for wires to a thermistor placed halfway along the probe. The applied measuring probes were 50 mm long with an outer diameter of 1.5 mm. The needle probe was inserted into the material of unknown thermal properties. For consolidated material, as measured here, small holes were drilled using high-speed drills. All samples were measured water-saturated. From the heating wire, with a very stable prescribed current, the probe supplies heat to the surrounding sample material with a constant power per unit length. From the temperature-rise function, measured at the center of the probe, thermal conductivity was determined by an iterative least-squares inversion technique as described by Kristiansen (1991). Probes were calibrated to standard materials of known thermal properties. For materials of good quality, the system operates with an accuracy of 3–5%. For further information on the AU needle probe system and recent methodology, we refer to Bording et al. (2019).

3.2.2. DH4 borehole

80 samples from the DH4 borehole were collected in June 2012 and thermal conductivity was measured with a Thermal Conductivity Scanner (TCS) at IRIS (Stavanger, now part of NORCE). The TCS optical scanning instrument has a measurement range of 0.2 to 25 W/m K with a reported accuracy and precision of 3% and a confidentiality of 95%. The method relies on optical laser heating of the sample surface and a standard using a mobile heat source and two infrared temperature sensors registering the temperature. Further details on the method are provided by Popov et al. (1999b) and Albert et al. (2017).

Samples from DH4 were first measured in the conditions they were sampled from core storage (i.e. dry state). When measurements of the dry samples were completed, the samples were saturated with a synthetic brine to make measurements that are comparable to natural in situ environments. Several of the shale samples from DH4 proved difficult to saturate with brine as the samples split parallel to lamination. For that reason, only ca. 50 of the original 80 samples could be measured in a brine-saturated state.

3.2.3. Determination of thermal conductivity from wireline logs

For Sysselmannbreen and DH4, parameter profiles of thermal conductivity and specific heat capacity were computed by applying prediction equations for sedimentary rocks developed by Fuchs et al. (2015). Digital log data, test data and lithological and stratigraphic information were implemented in the analysis. The logging data covered a broad range of standard well logs, from which gamma ray GR [API], density log RHOB [g/cm^3], sonic log DT [μs/m], photoelectric factor PE [-] and neutron log NPHI [-] were used for the thermal analysis. Depending on the depth-specific dominant sedimentary rock lithology (carbonates, clastic rocks, evaporates) and the petrophysical logs available for each depth section, a prediction equation was used reflecting the best combination of the available standard well logs and predictors derived from these. In this process, the volume fraction of shale VSH [-] was considered as linear gamma ray index. For the specific prediction equations, we refer to Appendix A–C in Fuchs et al. (2015)

3.2.4. Thermal conductivity from outcrop samples and publications

A research project focusing on the stabilization of the permafrost for geothermal wells and other infrastructure by thermosyphons was conducted and summarized in Daleng and Aftret (2021). Six outcrop samples were analyzed at NGU for thermal conductivity, of which five gave good results. The analyzed samples were from a Cretaceous dolerite dyke (Diabasodden Suite, sampled at Botneheia), cherts from the Upper Permian Kapp Starostin Formation (sampled in Sassendalen) and sandstone and sideritic sandstone from the Lower Cretaceous Carolinefjellet Formation (sampled near Longyearbyen). Thermal conductivity averages for five depth intervals are reported by Khutorskoy et al. (2013) for the Colesbukta borehole but unfortunately no details on the number of samples and determination of thermal conductivity is available.

3.3. Heat flow modelling

One-dimensional heat flow modelling was carried out on five different boreholes (Sysselmannbreen, DH1, DH4, Colesbukta and

Tromsøbreen-I), to quantify the spatial distribution of Svalbard's heat flow values (Nuus, 2020). The heat flow models were created using FiPy, which is a numerical partial differential equation solver integrated in Python (Guyer et al., 2009). The temperature distribution over time, with respect to depth of a given borehole can be found using FiPy which numerically solves the heat equation (eq.1), in which T is temperature, t is the timestep, z is depth, k is thermal conductivity, c is specific heat capacity, ρ is density, and S_u is radiogenic heat production.

$$\frac{\partial T}{\partial t} = \frac{k}{c\,\rho}\frac{\partial^2 T}{\partial z^2} + \frac{S_u}{c\,\rho}$$

To solve the heat equation, an initial temperature distribution, two boundary conditions and thermal rock properties are required. Thermal rock properties for the different boreholes, as well as radioactive heat production for different beds, were taken from Henne et al. (2014), summarized in Electronic Supplementary Material Table 6. These are based on thermal lab experiments of rock samples and later generalized based on lithology. The lithological logs of the boreholes are digitized and imported into the model, after which the respective lithologies are populated with the correct thermal rock properties.

The first boundary condition is a constant heat flow value at the base of the model and the second boundary condition is a fixed temperature at the top of the model. The value of the latter boundary condition is defined based on average temperatures from ice core data. The length of a model run is 800 000 years, of which the surface temperature will be set to −6 °C for the first 650 000 years and will vary according to constrained glaciations-interglacials for the last 150 000 years of the model run. The initial temperature distribution is linear from 180 °C at the base (6 km depth) to −6 °C at the top. The initial temperature distribution was chosen as it is closer to the final model outcome and the model will therefore converge sooner (Henne et al., 2014). At the end of the simulation, the modelled temperature curve was compared to borehole temperature data. Heat flow values were found by re-running the model for different heat flow values until the lowest RMS-error between the measured and modelled temperature curve was reached. This also made it possible to complement temperature curves for boreholes with sparse temperature data (e.g., Tromsøbreen-II).

4. Results

4.1. Regional perspective: Barents Shelf heat flow

Three main factors contribute to the regional thermal conductive configuration; the depth to the lithosphere asthenosphere boundary (LAB; equivalent to ~1300 °C), the upper crystalline crust and thick sediments via radiogenic heat production and the thermal insulation effect of porous sediments. Hence, the tectonic setting and its influence on these factors controls the regional thermal field. In the young oceanic domain, heat flow is mainly controlled by the depth to the LAB. Heat flow is highest in the vicinity of the mid-oceanic ridge and decreases with age of the oceanic lithosphere, as demonstrated in Fig. 1.

Long-lived subsidence in the Eastern Barents Sea and multiphase rifting in the SW Barents Sea led to the deposition of thick sediments and elevated thermal gradients in the respective basins. Rift-related faulting may allow fluid-controlled heat transport, locally superimposing the conductive thermal field in the SW Barents Sea. Anomalous heat flow may occur in the vicinity to salt pillows/diapirs as evident in, for instance, the Tiddlybanken, Nordkapp and Tromsø basins. Minor salt and anhydrite sequences are also mapped on the Kong Karl platform east of Svalbard while thick gypsum-anhydrite deposits with potential to influence the thermal gradients are exposed in central Spitsbergen and likely underlie the CSB.

A shallow continental LAB, attributed to ocean formation in the north and the west, results in higher lithospheric thermal gradients in the NW Barents Sea including Svalbard (Fig. 1). The effect of the shallow LAB is counteracted by multiple phases of uplift, glaciations and the absence of porous sediments. Young relatively porous sediments are mainly restricted to the CSB. However, the recent episodes of erosion and glaciation may imply that this region is still in a transient thermal state, as also evidenced by out-of-equilibrium pressure regimes (Birchall et al., 2020), ongoing uplift (Kierulf et al., 2022; Lasabuda et al., 2021) and recent volcanism in north-western Spitsbergen (Gjelsvik, 1963).

4.1.1. Offshore petroleum exploration boreholes

Offshore petroleum exploration boreholes are in the area open to petroleum exploration south of Bjørnøya, relatively far away from the study area. For the sake of completeness, we nonetheless briefly report on heat flow determinations carried out with petroleum industry data.

Pascal (2015) elaborated an original approach to compute heat flow from incomplete petroleum industry datasets and applied it to the Norwegian Continental Shelf, including the south-western Barents Sea. Thirteen boreholes were found suitable for computations, yielding heat flows between 65 and 83 mW m^{-2} and a median value of 72 mW m^{-2} with a standard deviation of 5 mW m^{-2}. Assuming Pliocene to Quaternary deep erosion (i.e. up to 1 km), heat flow values were most likely overestimated by 4 to 10 mW m^{-2}. Nevertheless, the results point to relatively high heat flow values in the entire south-western Barents Sea. Furthermore, Pascal (2015) suggested increasing heat flow westwards, compatible with lithosphere thinning from the cratonic lithosphere of the eastern Barents Sea towards the young oceanic basement of the north-eastern Atlantic.

To note, the previous values of heat flow from the SW Barents Shelf appeared to be higher than the ones gathered in shallow drillholes in the 1980s (Løseth et al., 1993; Sættem, 1988; Zielinski et al., 1986). These were found to range from 54 mW m^{-2} to 73 mW m^{-2} and resulted in median and standard deviation values of 65.5 mW m^{-2} and 7 mW m^{-2} respectively (Pascal, 2015).

4.1.2. Marine heat flow stations around Svalbard

Near Svalbard, marine heat flow data were primarily acquired above oceanic basement and reflect the expected decrease of heat flow with lithosphere age (Sundvor et al., 2000). Limited data were acquired on the continental shelf of Svalbard (see discussion in Pascal, 2015). Amongst these, three measurements were taken north-east of Svalbard by Crane et al. (1982). One of the measurements was of poor quality and the two other ones yielded moderate heat flows of 57 and 61 mW m^{-2}, respectively. However, the data were acquired at relatively shallow depths below sea level and were presumably affected by short-term variations in bottom water temperature.

The ~E-W marine heat flow profiles of Crane et al. (1988) covers mostly oceanic crust and the continent-ocean boundary (COB) west of Svalbard. The values reported by the authors (see also Sundvor, 1986; Sundvor et al., 1989) suggested high heat flows up to 100 mW m^{-2}, yet thermal gradients were difficult to establish for some sites. The assumption of high heat flows seems to be supported by the results obtained along a profile taken following parallel 78 °N. Note that at the specific location of the profiles the Knipovitch Ridge is located only ~50 km from the COB and large amounts of heat are expected to be transferred laterally to the continent.

Soviet and later Russian researchers have conducted offshore heat flow measurements around Svalbard and linked these to large-scale structures and recent seismicity (Antonovskaya et al., 2018).

4.2. Borehole temperature data

Deep (i.e. > 200 m) borehole temperatures are recorded below the permafrost in exploration and research boreholes throughout Svalbard and exhibit a spatial variation in geothermal gradients (Fig. 2). These range from 24 °C/km at Sarstangen in Cenozoic strata in western Spitsbergen to 53 °C/km at Tromsøbreen-I in Mesozoic strata in southern Spitsbergen. The high lateral variability is also evident in the CSB,

with geothermal gradients of 30 °C/km (Colesbukta) and 28 °C/km (Reindalspasset) increasing to 36 °C/km (DH2) and 43 °C/km (DH4) at distance of approximately 20 km. In shallow sediments, such as offshore Oregon, significant variation (50% increase) in heat flow was observed at distances of 1–2 km and attributed to topographic effects, with a component of warm fluids migrating upwards along faults (Ganguly et al., 2000). Long-lived faults are also present within Svalbard and may explain some of the spatial variation, though for instance both the Sarstangen and Tromsøbreen boreholes locate near the WSFTB and display a significantly different geothermal gradient. The heterogeneous sedimentary cover with variable thermal conductivity and large lateral variations in uplift magnitude, reflected also in source rock maturation increase westwards (Olaussen et al., 2023), will also influence the heat flow and further work is required to constrain the controlling mechanisms for such large variation in heat flow onshore Svalbard.

A compilation of temperature-depth data (Fig. 4) confirms this variable trend. However, it also illustrates that the two boreholes at Tromsøbreen exhibiting high geothermal gradients (> 45 °C/km) are outliers. The other boreholes all show more "normal" geothermal gradients not exceeding 35 °C/km. Overall, borehole temperature data including all boreholes suggest an average geothermal gradient of 33 °C/km, while excluding the two Tromsøbreen boreholes gives an average of 30 °C/km.

It is notable that many boreholes only offer limited or even single bottom hole temperatures (BHT), with strong uncertainty on the effect of drilling on the measurements.

For the research boreholes, where wireline temperature data are available in addition to BHT, we have calculated average geothermal gradient with a running mean over 20 m and 100 m depth windows (Fig. 5). These illustrate geothermal gradients ranging from 9 °C/km to 68 °C/km with a clear correlation to lithologies. The highest gradients are calculated for shale-dominated sections.

4.2.1. Shallow permafrost borehole observations

Measurements at Janssonhaugen by Isaksen et al. (2000) indicate a geothermal gradient of 36 °C/km (heat flow at 65 mW/m^2) at the bottom 20 m interval within the 102 m deep borehole fully affected by permafrost. In the lower Endalen 100 m deep borehole the geothermal gradient is around 5 °C/100 m, and the permafrost thickness is around 120 m based on this gradient. In general, in central Spitsbergen the permafrost temperatures vary from −2 °C to −6 °C at 20 m depth.

4.3. Physical rock properties and borehole temperatures onshore svalbard

Svalbard's stratigraphic record offers opportunities for systematically deriving physical properties for thermal modelling from drill cores and outcrops. Here we present and discuss new data on thermal conductivity from four research boreholes (DH1, DH2, DH4 and Sysselmannbreen), and relate these to measured temperature profiles. In addition, we provide thermal conductivity measured on undrilled rock samples from surface outcrops by Daleng and Aftret (2021).

4.3.1. Thermal conductivity

Fig. 6 synthesizes all thermal conductivity data measured on Svalbard's drill cores and field samples, sorted by stratigraphy and lithology (see Electronic Supplementary Material Table 7 for data). The same data are also plotted as a histogram (Fig. 7), giving a bimodal distribution with shales of consistently lower thermal conductivity (mean = 2.31 W/m K, $n = 143$) than sandstones (mean = 3.92 W/m K, $n = 89$). Shales and siltstones have thermal conductivity from 1.6 to 3.5 W/m K. Sandstones have a wider spread, ranging from 2.1 to 6.5 W/m K.

Thermal conductivity measurements are consistent between drill cores and outcrop samples, as illustrated by the Carolinefjellet Formation (Fig. 7). Thermal conductivity is highest in the sandstones but is also high (4.5 W/m K.) in the Late Permian spiculitic Kapp Starostin Formation.

4.3.2. Sysselmannbreen

Thermal properties were measured on 95 core samples evenly distributed in the Sysselmannbreen borehole (Fig. 8). 61 samples of shales and siltstones were measured by AU and 34 samples of sandstones were measured by NGU (Electronic Supplementary Material Table 7). The measurements resulted in average and median thermal conductivity of 2.2 W/m K for the shales/siltstones with a modest standard deviation of 0.25 W/m K. The measurements of sandstone samples yielded average and median thermal conductivities of 4.0 and 3.7 W/m K, respectively, and a relatively large standard deviation of 0.75 W/m K. The measured sandstones were rather heterogeneous, hence variable coal and shale

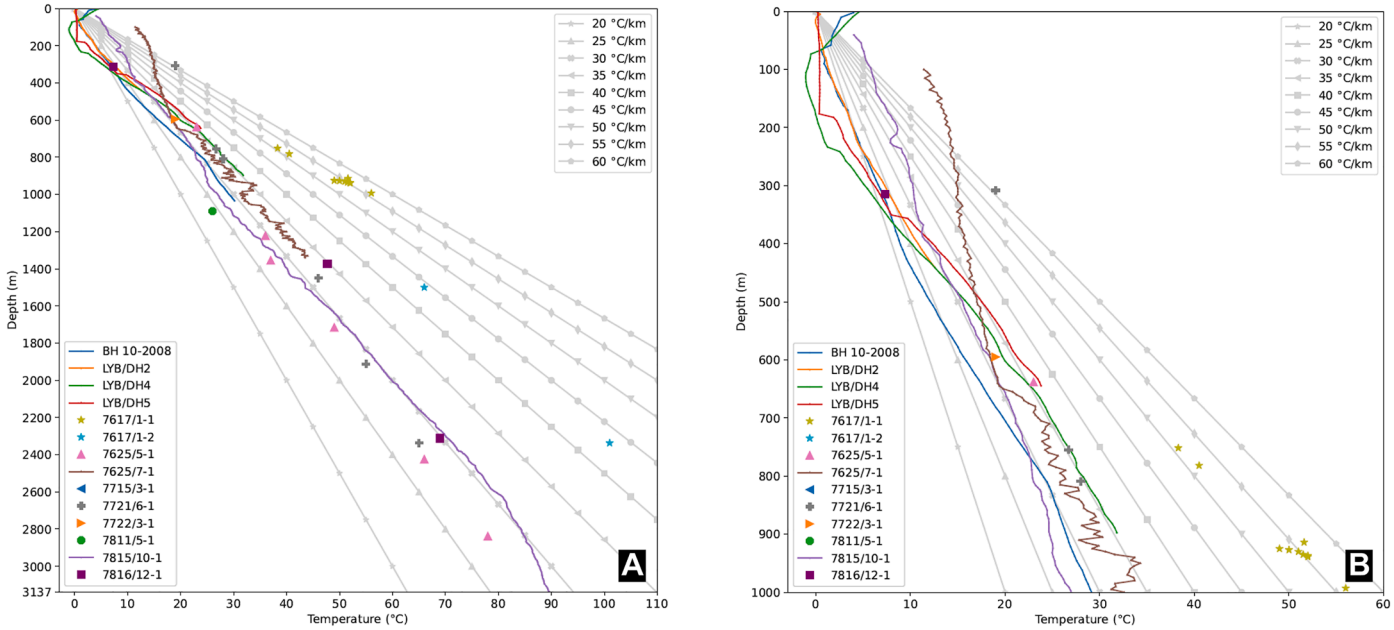

Fig. 4. Temperature versus depth for all Svalbard boreholes. All data are plotted in A), while only the uppermost 1 km is plotted in B). Temperature gradients in the shallow subsurface are strongly affected by the permafrost (i.e. temperature < 0 °C for over 2 years).

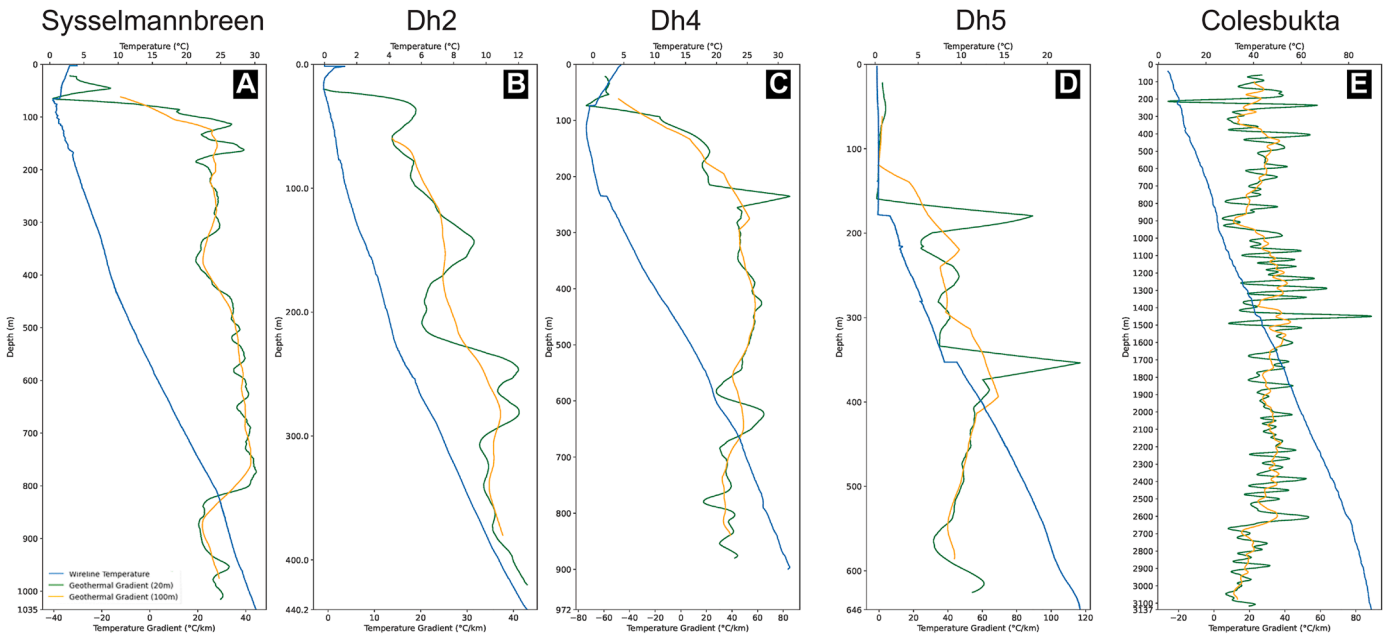

Fig. 5. Wireline temperature data with calculated geothermal gradients for a) Sysselmannbreen, b) DH2, c) DH4, d) DH5 and e) 7815/10–1 Colesbukta. Geothermal gradients were calculated over a 20 m and 100 m depth window.

additions to the quartz-dominated matrix was probably the cause for such relatively large standard deviation. Relatively high thermal conductivities of > 5 W/m K were also measured for the sandstones (Fig. 8). These latter values were judged realistic, considering the low porosities that characterize the largely cemented formations penetrated in the Sysselmannbreen borehole (i.e. from 3% to 10%; Elvebakk et al., 2008).

4.3.3. DH1

Thermal properties were measured on 57 core samples evenly distributed in the DH1 borehole (Fig. 9). Seven sandstone samples, gathered from deeper intervals in the neighboring DH2 borehole, were added, bringing up the total number of measured samples to 64. DH2 is located only 30 m away from DH1 and no significant geological variation was detected between the two wells (Elvebakk, 2008). In summary, 17 samples of shales and siltstones and 46 samples of sandstones and conglomerates from the DH1 borehole were measured by AU and NGU respectively (Electronic Supplementary Material Table 7). Additionally, one sample of coal from DH1, measured at NGU, returned a thermal conductivity value of 1.3 W/m K.

Amongst the collection of sandstones/conglomerates, two samples yielded unrealistically high conductivity values of 7.5 and 8.3 W/m K (Electronic Supplementary Material Table 7). Inspection of the samples showed that one sample was severely damaged, and that the other contained relatively high amounts of sulphides. These specific samples were consequently discarded from the analysis.

The measurements of the remaining 44 samples of sandstones/conglomerates resulted in average and median values of 3.8 and 3.5 W/m K, respectively, with a standard deviation of 1.2 W/m K. Similar to the Sysselmannbreen borehole, the relatively large scatter of thermal conductivity values was attributed to composition heterogeneity, and the relatively high conductivity values to the low porosities measured for the penetrated formations (i.e. between 5% and 10%; Elvebakk, 2008).

The thermal conductivity measurements carried out on the shales/siltstones yielded average and median values of 2.2 W/m K and a standard deviation of 0.4 W/m K. The latter values were remarkably similar to the ones found for the Sysselmannbreen shale/siltstone samples.

In conclusion, the measurements delivered realistic thermal conductivity values for the two types of lithologies (i.e. shale and quartz dominated rocks) encountered in the Sysselmannbreen and DH1 (and DH2) boreholes. Although porosity of the penetrated formations was rather low, its effect was included in our measurements. Temperature corrections were not implemented but these were deemed negligible in the present case, considering the shallow penetration depths of the studied boreholes (i.e. maximum ~ 1 km depth below ground surface). Our measurements were not corrected for pressure effects and the measured values might slightly underestimate in situ thermal conductivities, especially at great depths in the boreholes. We note that the effects of temperature and pressure generally have the opposite effect; increasing temperature reduces thermal conductivity and increasing pressure increases conductivity, thus, to some extent, cancel each other out when only sedimentary rocks are considered.

4.3.4. DH4

80 thermal conductivity values are available for DH4, with the majority in the lower half of the borehole (Fig. 10). The highest thermal conductivity is in the sandstones of the Helvetiafjellet Formation (5.1 W/m K), while the lowest thermal conductivity is in the organic-rich shales of the Agardhfjellet Formation (1.8 W/m K). Below the permafrost-affected uppermost ca 120 m, the geothermal gradient is roughly 40 °C/km. Locally the geothermal gradient increases in shaly intervals and decreases in sandy intervals, as also correlated with the gamma ray log (Fig. 10).

4.3.5. Colesbukta

Thermal conductivity is available from the petroleum exploration borehole at Colesbukta from a publication (Khutorskoy et al., 2013), but there are no details on individual measurements. Thermal conductivity is reported as averages for five depth sections, with values of 2.24 W/m K (460–670 m), 2.35 W/m K (960–1220 m), 2.48 W/m K (1620–2100), 2.35 W/m K (2110–2460 m) and 1.99 W/m K (2530–2630 m). Furthermore, the borehole offers the most comprehensive deep temperature data onshore Svalbard to 3137 m depth. The calculated geothermal gradient is largely controlled by lithology (Fig. 11).

4.4. Anisotropy of thermal conductivity

Thermal conductivity was measured in both horizontal and vertical

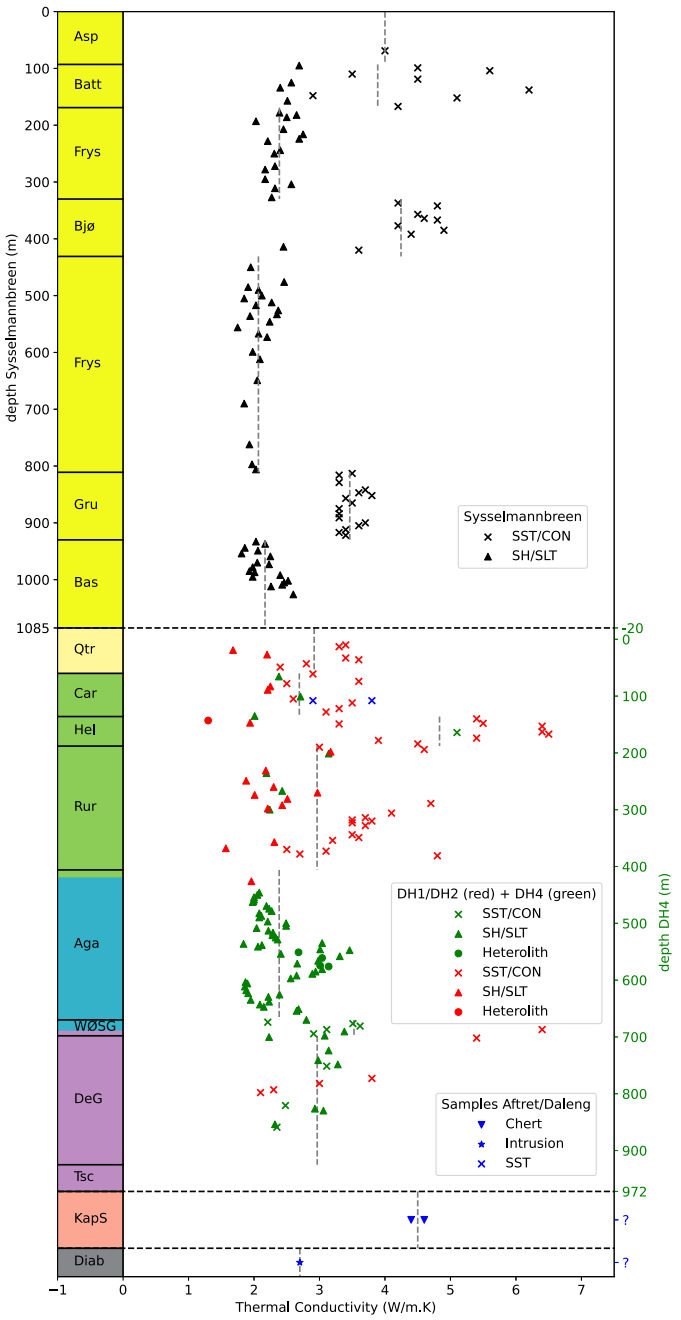

Fig. 6. Compilation of all available thermal conductivity data from Svalbard, sorted by stratigraphic position. DH1 and DH2 data are shifted upwards to account for the regional geological dip and fit the DH4 depth scale. Outcrop samples of the Carolinefjellet and Kapp Starostin formations and the Diabasodden Suite from Daleng and Aftret (2021) were included for completeness. Formation abbreviations and average thermal conductivity (in W/m K): Asp = Aspelintoppen (4.00), Batt = Battfjellet (3.89), Frys = Frysjaodden (upper part: 2.39, lower part: 2.07), Bjø = Bjørnsonfjellet Member (4.25), Gru = Grumantbyen (3.46), Bas = Basilika (2.17), Qtr = Quaternary valley fill (2.92), Car = Carolinefjellet (2.69), Hel = Helvetiafjellet (4.83), Rur = Rurikfjellet (2.96), Aga = Agardhfjellet (2.38), WØSG = Wilhelmøya Subgroup (3.52), DeG = De Geerdalen (2.96), Tsc = Tschermakfjellet (no data), KapS = Kapp Starostin (4.5), Diab = Diabasodden Suite igneous intrusions (2.7).

directions on 79 samples from DH4, allowing the plotting of anisotropy of thermal conductivity for both water-saturated and dry samples (Fig. 12). This was motivated by previous work, for instance Simmons (1961) and Midttømme and Roaldset (1999) who suggested that in some cases thermal conductivities measured parallel to bedding appears to be more than twice of that measured perpendicular to bedding. Our data show a relatively good fit of horizontal to vertical thermal conductivity. Interestingly, horizontal thermal conductivity slightly exceeds vertical thermal conductivity at conductivities below ca. 3 W/m K. Above 3 W/m K, this is opposite. This could be related to the experimental conditions leading to secondary opening or due to little or no pressure added during the measurements, which we relate to secondary non in situ effects.

4.5. *Thermal conductivity from wireline logs*

Thermal conductivity was also derived from borehole wireline logs, following the method presented by Fuchs et al. (2015). Calculated curves for the Sysselmannbreen and DH4 boreholes are shown in Fig. 13. There is strong agreement with the drill core plug-derived thermal conductivity throughout most of the succession, with the exception of the under-estimated thermal conductivity for the Helvetiafjellet Formation sandstones in the overburden.

4.6. *Temporal temperature data: Adventdalen*

Downhole temperatures are typically recorded soon after drilling, which may influence the measurements. In the upper 440 m of DH1 and DH2 in Adventdalen temperatures were also recorded using fibre optic cables 7 years after drilling (Fig. 14). The temperature in the lower section of the borehole has decreased by 0.4–0.8 °C in the 7 year period (Fig. 14). This is assumed to be due to the temperature instability and the injection of heat during drilling. The comparison of the temperatures measured in the DH1 and DH2 boreholes in 2014 is consistent at depths over 80 m (Fig. 14C), unsurprising given the short distance between the two boreholes.

4.7. *Heat flow models*

Five wells were strategically chosen for initial 1D heat flow modelling (Fig. 15). The wells penetrate variable stratigraphy and are also geographically widespread (Fig. 2). The Sysselmannbreen borehole in the youngest part of the stratigraphy suggests heat flow of 76 mW/m^2. The other three wells overlying the CSB, DH1, DH4 and Colesbukta, penetrate deeper stratigraphy and converge to heat flow of 66 mW/m^2, 71 mW/m^2 and 48 mW/m^2, respectively. The anomalously high heat flow values of 96 mW/m^2 are derived from the Tromsøbreen II well.

These heat flow values were inverted for by assigning thermal conductivity, heat capacity, density and radioactive heat production to different lithologies found throughout the log. For siliciclastic material, these values from Henne et al. (2014) (Electronic Supplementary Material Table 6) were used. The carbonate rocks were given a thermal conductivity value based on laboratory conductivity measurements on samples from central Spitsbergen (Daleng and Aftret, 2021). Density and radiogenic heat production were assigned approximated values of 2700 kg/m^3 (Joshua et al., 2008) and 0.07 μW/m^3 (McKenna and Sharp, 1998) based on laboratory experiments outside of Svalbard. Heat capacity was assigned the same value assumed as all the siliciclastic rocks, which was 850 J/kg K, since Henne et al. (2014) suggested that this was one of the less influential parameters. A temperature curve is then constructed using these parameters and after applying constant heat flow at the base of the model. The heat flow is adjusted until the lowest RMS-error with the actual temperature measurements was found.

Lithological variation with depth used model the heat flow for DH4 and Sysselmannbreen is the same as used by Henne et al., 2014 (Electronic Supplementary Material Table 6). For DH1, Tromsøbreen-II and Colesbukta, sedimentary logs from boreholes were discretized (e.g., Olaussen et al., 2019 for DH1 and DH4). For DH1, a separate heat flow model was constructed in which average values for thermal conductivity per formation were used (Fig. 6), while the remaining heat capacity, density and radioactive heat production still depend on the lithology

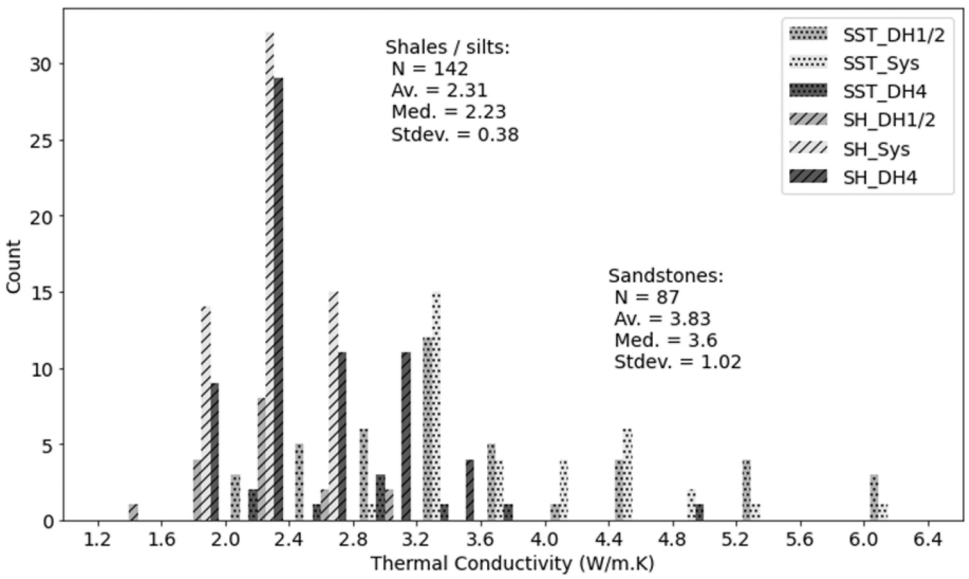

Fig. 7. Distributions of thermal conductivities measured on drill core samples from DH1 and DH2 ("DH1/2"), DH4 and Sysselmannbreen ("Sys"). Average (*Av.*), median (Med.) and standard deviation (Stdev.) values are given for the two dominant types of lithologies, shales and sandstones. Bins are indicated by values on x-axis (e.g., first bin is between 1.2 and 1.6 etc.).

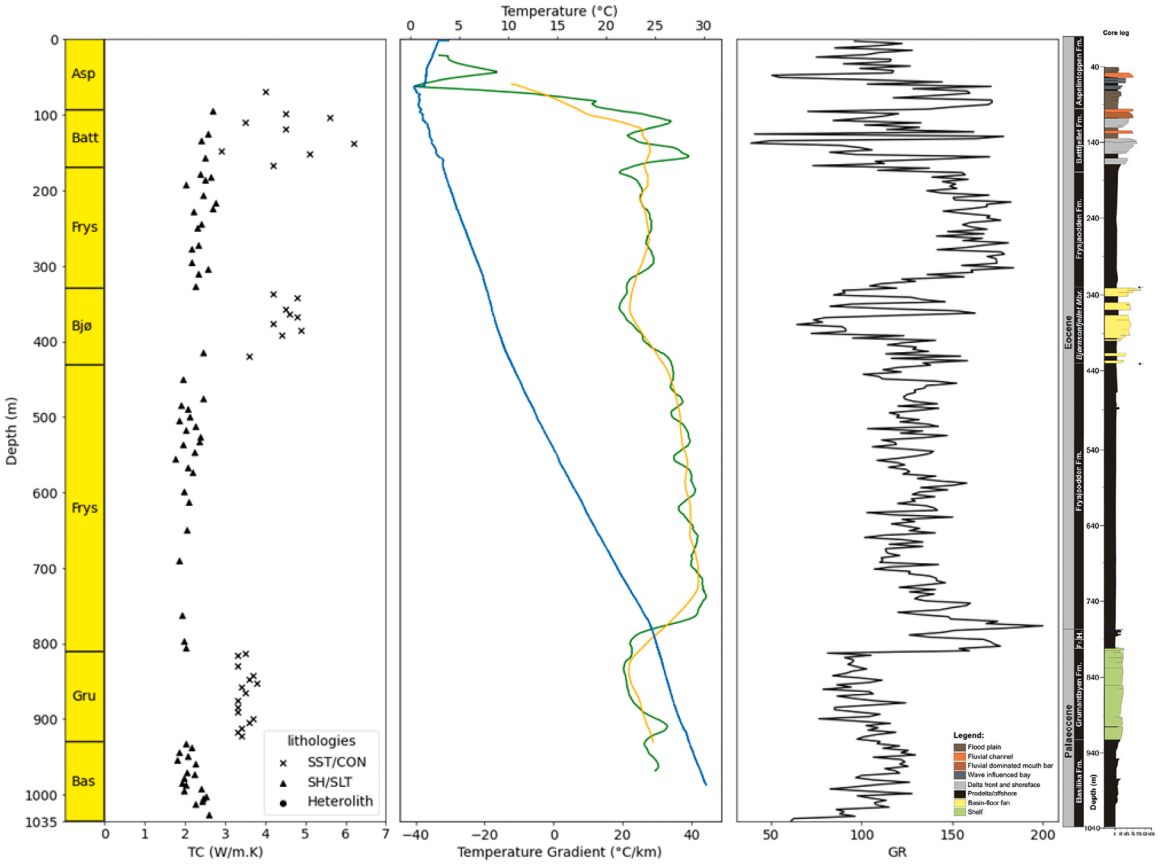

Fig. 8. Stratigraphy, lithology, thermal conductivity, wireline temperature, calculated geothermal gradients and the gamma ray log from the Sysselmannbreen borehole. For formation names refer to Fig. 6. The sedimentary log is from Grundvåg et al. (2014).

from a discretized log. A significantly higher heat flow value of 99 mW/m^2 was found in this instance, resulting from higher thermal conductivity values ranging from 2.38 to 4.83 W/mK.

For boreholes with more recent wireline temperature measurements such as DH4 the measurement uncertainties are known. For the older boreholes with sparse temperature measurements (e.g., Tromsøbreen-I), these uncertainties are not known. Trying to fit a temperature curve to a sparse number of points with unknown uncertainty therefore also results in a larger uncertainty of the approximated heat flow value.

The results show values exceeding 70 mW/m^2 within the CSB (DH4

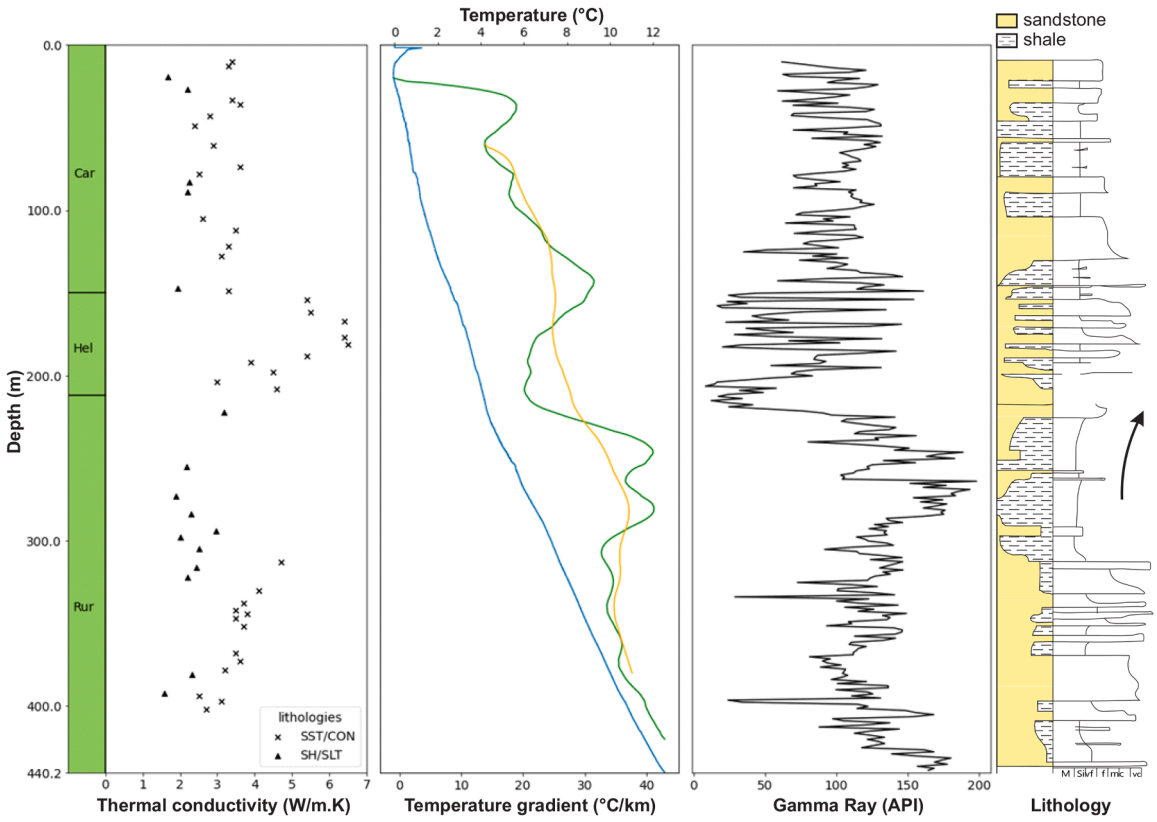

Fig. 9. Stratigraphy, lithology, thermal conductivity, wireline temperature, calculated geothermal gradients and the gamma ray log from the DH1/2 borehole (first 440.2 m). For formation names refer to Fig. 6. The sedimentary log is from Olaussen et al. (2019).

and Sysselmannbreen) and up to 96 mW/m^2 for Tromsøbreen II. Previous work by Pascal et al. (2010a) and Henne et al. (2014) show similar modelled heat flow values, varying between 60 and 80 mW/m^2. The higher heat flow values compared to those found in mainland Norway are attributed to a thinned lithosphere below the Svalbard archipelago (Beka et al., 2015). Still, the large spatial variation in heat flow even within onshore Spitsbergen is intriguing.

4.8. Longyearbyen geothermal well prognosis

As part of the deep geothermal feasibility project led by SNSK in 2021–2022, Olaussen and Birchall (2022) provide a detailed well prognosis to 2000 m depth for the Longyearbyen area. The prognosis, illustrated in Fig. 16, combines the stratigraphy penetrated by the almost 1 km deep DH4 borehole in Adventdalen (Olaussen et al., 2019 and references therein) with regional geological knowledge about the deeper part of the stratigraphy from outcrop studies and petroleum exploration boreholes (Olaussen et al., 2023).

The uppermost 100 m of the proposed well comprise Quaternary marine, glacial, sub-glacial and fluvial sediments. Coarse glacial boulders up to dm-scale represent drilling challenges. The area is heavily affected by permafrost, ranging from ca 120 m thickness at the DH4 borehole to <30 m near the coast. Natural gas and artesian water are present just beneath the permafrost, posing a drilling hazard.

Theectionn from 100 to 1400 m depth comprises Mesozoic siliciclastic deposits. The sandstones-siltstones-shales are locally intruded by Early Cretaceous dolerite sills of up to 50 m thickness. Furthermore, two major regional decollement zones occur in this interval, specifically within the Agardhfjellet and Botneheia formations (Fig. 16). Severe underpressure (Birchall et al., 2020) and the presence of shale gas (Ohm et al., 2019) must be considered when drilling or assessing the predictability of fluid flow, which will have implications on open system geothermal flow.

The Permian-Triassic boundary is expected at around 1400 m depth. An approximately 200 m thick chert-dominated succession with minor carbonates is present beneath this major boundary that also marks a strong shift in the mechanical competence of the strata. Overpressure is unlikely, but may be encountered in this section. The lowermost part of the prognosed well, from 1600 to 2000 m, comprises carbonates and evaporites, with the Wordiekammen Formation exhibiting zones of strong fluid flow potential.

The lowermost decollement zone occurs in Permian evaporites. It is possible that the numerous decollement zones represent zones of weakness and the potential for clay swelling, which must be considered in wellbore stability calculations.

Subsurface temperature is well constrained in the uppermost 1 km covered by the DH4 borehole, which offers 31.6 °C at 899.6 m and an average geothermal gradient of 40 °C/km (Figs. 2 and 4). Deeper down at 2 km the temperatures are not measured. Extrapolation of the DH4 geothermal gradient would suggest temperatures of around 79 °C. Lateral extrapolation of deep petroleum exploration boreholes suggest lower temperatures around 55–60 °C at 2 km depth. The 7811/5–1 Colesbukta borehole 19 km south-west of Longyearbyen measured 60 °C at 2 km, while the 7816/12–1 Reindalspasset borehole 36 km south-east of Longyearbyen measured 55 °C at 2 km (Fig. 4).

5. Discussion

5.1. Spatial variations in heat flow

Fig. 2 illustrates the significant present-day variability in average geothermal gradients from exploration boreholes, and the main structural elements such as faults that may influence heat flow. However, the different well depths and local stratigraphy also influence the

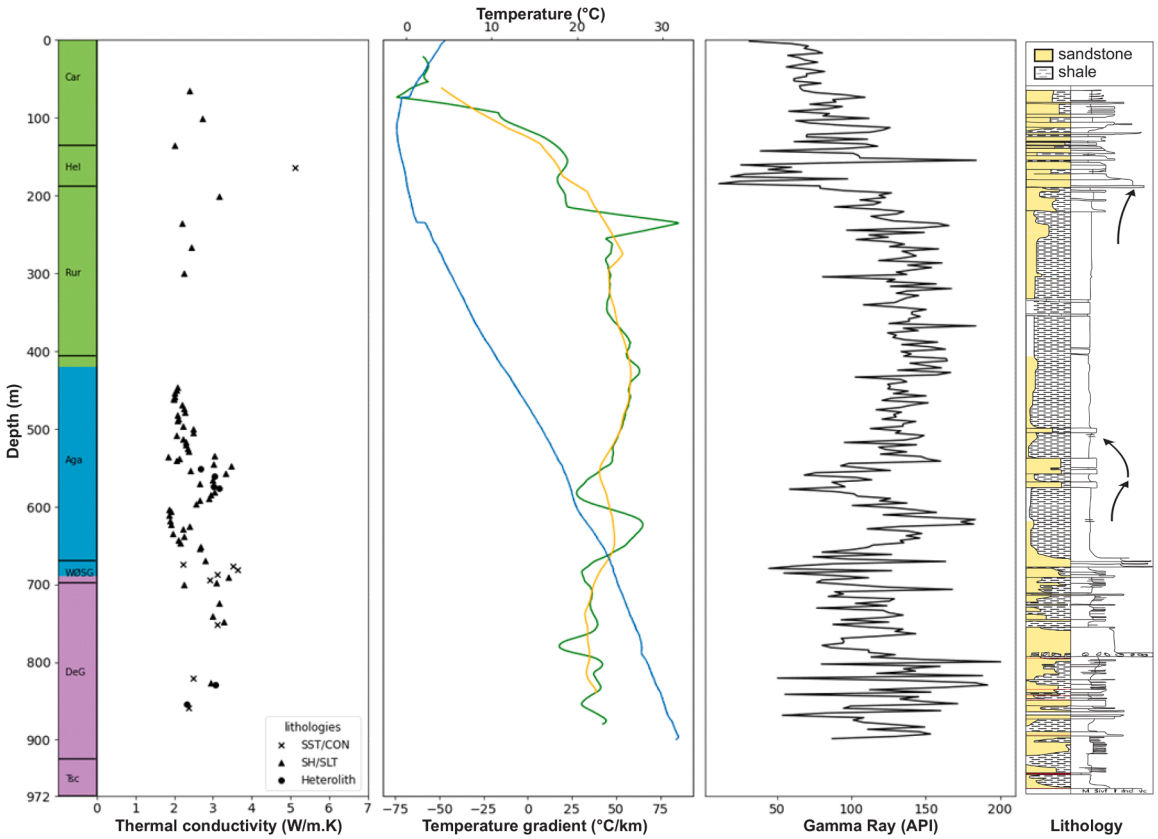

Fig. 10. Stratigraphy, lithology, thermal conductivity, wireline temperature, calculated geothermal gradients and the gamma ray log from the DH4 borehole. For formation names refer to Fig. 6. The sedimentary log is from Olaussen et al. (2019).

variability. To disentangle some of these factors we plot the measured and extrapolated temperatures at different depths (1, 2, 3, 5 and 10 km) in Fig. 17.

The most anomalous area is centered on the Tromsøbreen-I borehole, with geothermal gradients of 55 °C/km. The area is near major fault systems, both faults associated with the West Spitsbergen Fold and Thrust Belt and deeper-rooted N-S lineaments described above. Both may be candidates for locally enhancing convective heat transfer and anomalous heat flow values. The deeper Tromsøbreen II borehole drilled in the immediate vicinity exhibits geothermal gradients of "only" 43 °C/km, possibly implying that temperatures were overestimated and still affected by drilling activity.

Limited crustal-scale thermal modelling is available from Svalbard, partly due to the lack of crustal scale refraction seismic data. Klitzke et al. (2016) conduct lithosphere-scale thermal modelling across the entire Barents-Kara Sea. The model, however, is too coarse to adequately describe the lateral thermal variation onshore Svalbard. Neither are the deep exploration boreholes presented in this study included in the model.

This is also the case for the regional thermal modelling transect across southern Svalbard by Grad and Majorowicz (2020). Fig. 18 illustrates the profile location, crustal structure and thermal model along the 800 km long regional profile from the mid-ocean ridge to the Edgeøya Platform. The transect is aligned with an onshore-offshore seismic refraction profile and crosses near the Tromsøbreen I thermal anomaly.

Further afield, Chen et al. (2018) investigates the geological controls on subsurface temperatures in the Canadian Sverdrup Basin using 119 petroleum exploration boreholes. Geothermal gradients in the Sverdrup Basin vary as in Svalbard, with 18 °C/km to 39 °C/km reported from 11 boreholes by Jones et al. (1990) and 15 °C/km to 50 °C/km reported from 156 wells by Majorowicz and Embry (1998). The Sverdrup Basin shares much geological history with Svalbard, including emplacement of HALIP intrusions and Eocene uplift during the Eurekan orogeny. However, neither of these events appear to influence present-day thermal regime, with past thermal anomalies having dissipated (Chen et al., 2018). The two major thermal regimes recognized by Chen et al. (2018) rather relate to lithologies – with the high temperature regions correlating with salt structures and low temperature regions with exposed Mesozoic aquifers affected by recent sub-glacial and meteoric recharge.

5.2. *Temporal variations in heat flow and paleoclimate temperatures*

Past heat flow variations are tied to the geological evolution, as outlined above. The most significant events include circum-Arctic magmatism during the emplacement of the HALIP-related igneous intrusions and recent uplift (Lasabuda et al., 2021). However, as pointed out by Chen et al. (2018) for the Sverdrup Basin, these local temperature anomalies are likely dissipated by the present day. Paleo-geothermal gradients in the Sverdrup Basin are estimated to be slightly lower (mean 28 °C/km) than present day (mean 31 °C/km) by Majorowicz and Embry (1998). This minor difference may well be within the uncertainty limits of the measurements.

In deeper boreholes elsewhere, including the Kola superdeep borehole SG-3 (12 262 m deep) in Russia (Popov et al., 1999a) and the fully cored Outokumpu deep (2516 m) borehole in Finland (Kukkonen et al., 2011), older temperatures are recorded in heat flow. If good data are available, including high-resolution thermal conductivity data and downhole temperatures measured long after drilling, one can invert heat flow data for past ground surface temperatures and thus gain quantitative insights into paleotemperature evolution. Kukkonen and Joeleht (2003) conduct this for the Fennoscandian Shield and the East European Platform and suggest that Weichselian (i.e. Late Pleistocene) glaciation temperatures are recorded in deep (> 1000 m) boreholes. Maystrenko

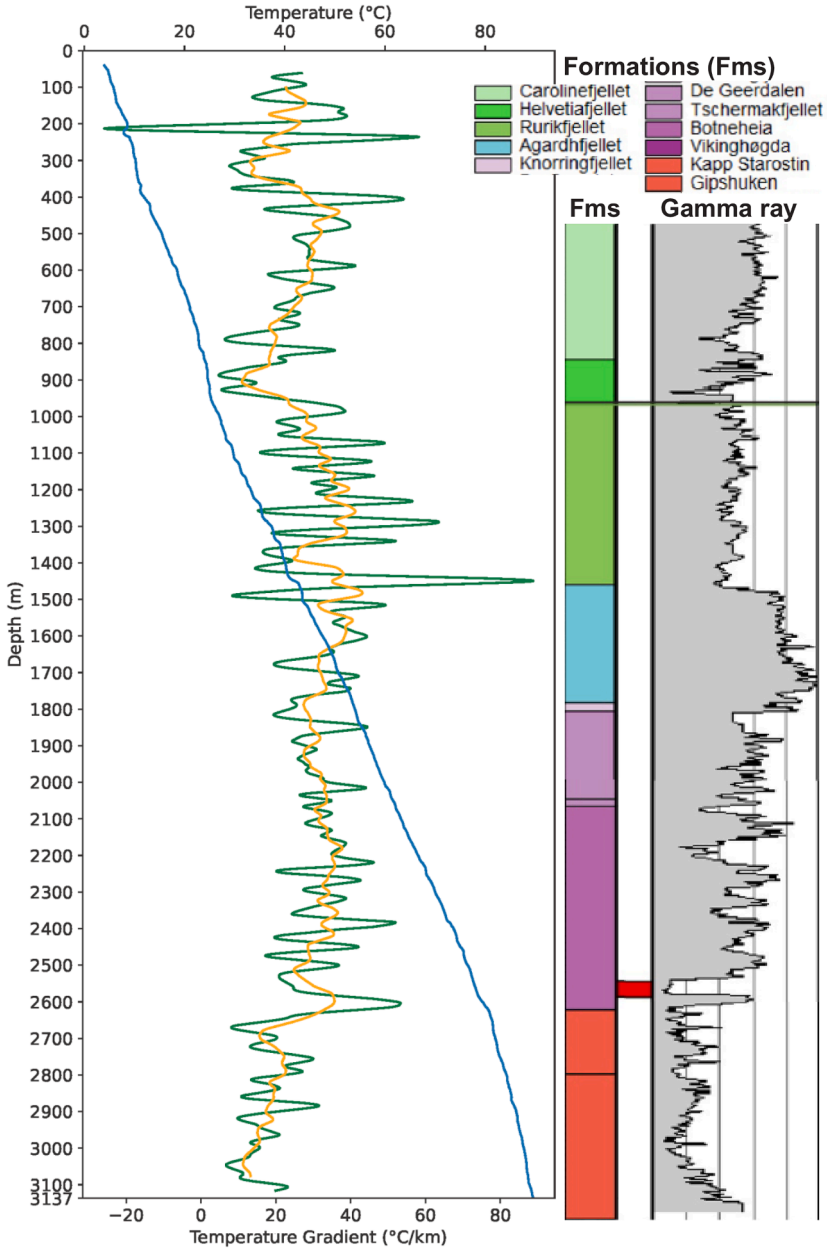

Fig. 11. Temperature, temperature gradients and gamma ray for the Colesbukta borehole. The formation boundaries and gamma ray log are from Senger and Galland (2022).

et al. (2021) use two deep boreholes to recognize a relatively strong paleoclimatic signal down to a depth of 2000 m from mid-Norway, depending on the thermal conductivity of the bedrock. In Fennoscandia the paleoclimate effect can be up to 20 mW m^{-2} (Majorowicz and Wybraniec, 2011; Maystrenko et al., 2021).

In Svalbard, such an exercise is tempting but is hampered by the lack of high-quality high-resolution thermal conductivity data from boreholes deeper than the 972 m deep DH4 borehole. The two deepest boreholes in Svalbard, Ishøgda (3304 m) and Colesbukta (3173 m), unfortunately do not provide any thermal conductivity measurements, beyond depth-window averages for the Colesbukta borehole (Khutorskoy et al., 2013), and only fragmented downhole temperature measurements. However, the planned deep geothermal borehole near Longyearbyen may represent an opportunity to conduct follow-up studies including quantification of the paleoclimate effect.

5.3. *Thermal effects of erosion and deposition*

Multiple major uplift events have impacted the Barents Shelf throughout the Cenozoic (Henriksen et al., 2011; Nyland et al., 1992), resulting in kilometer-scale erosion and re-deposition of sediments throughout the region (Fiedler and Faleide, 1996; Lasabuda et al., 2021; Medvedev et al., 2023). Arguably the most important of these events is the ongoing cycles of glacial and interglacial conditions, which began some 3.5 million years ago (Knies et al., 2009; Solheim et al., 1998). Abnormal sub-hydrostatic pressures occur at shallow depths throughout the northern Barents Shelf (Birchall et al., 2020) and the prevalence of thermogenic shallow gas (Ohm et al., 2019; Senger et al., 2019) demonstrate that the current pressure and volume conditions are likely in a transient state. Estimated maturation of Middle Triassic and Upper Jurassic organic rich marine mudstone and quartz diagenesis of Mesozoic sandstones (Olaussen et al., 2023) probably reflect both variation in the magnitude of the late Neogene uplift magnitude and the fluctuations

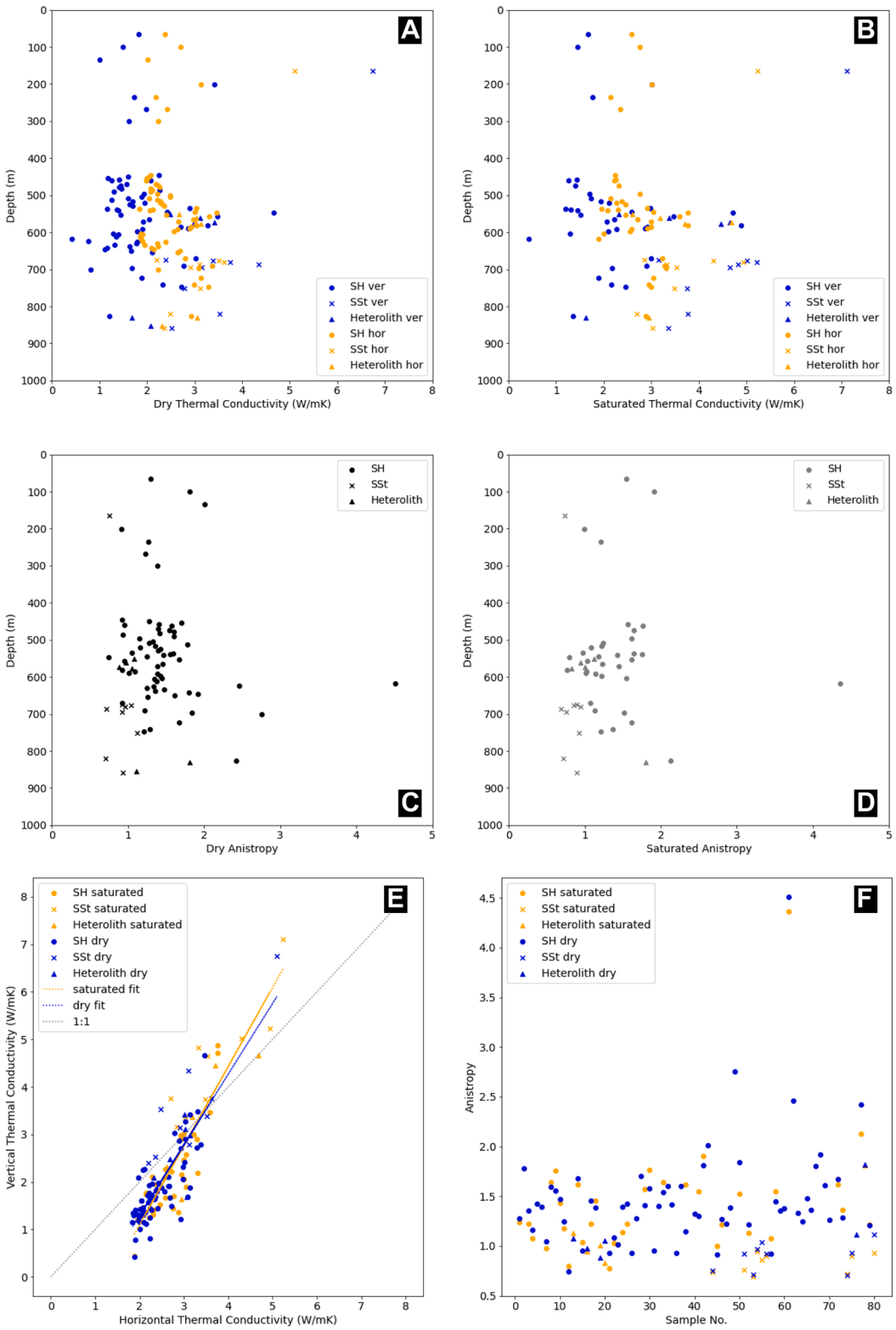

Fig. 12. Overview of anisotropy of thermal conductivity from the DH4 borehole. A) and B) Depth vs horizontal and vertical thermal conductivity in dry and brine-saturated state, respectively. C) and D) Anisotropy versus depth, for dry and brine-saturated state, respectively. E) Vertical vs horizontal thermal conductivity (color-coded by lithology/well). F) Sample No. vs Anisotropy (color-coded by lithology/well). Data are provided in Electronic Supplementary Material Table 8.

of past and present geothermal gradients. Reconstructions indicate that central and western Spitsbergen were uplifted by nearly 2.5 to 3 km in the late Neogene (Lasabuda et al., 2021; Olaussen et al., 2019) and still rise 9 mm/year (Kierulf et al., 2022). Only 1 mm/year uplift is linked to isostatic rebound formed due to the last glacial period, i.e., Late Weichselian glaciation (Kierulf et al., 2022). This differential uplift might be connected to active tectonics as supported also by recent seismicity (Minakov, 2018).

The impacts of these uplift events on the thermal regime would likely have been significant and complex. On a fundamental level, uplift and

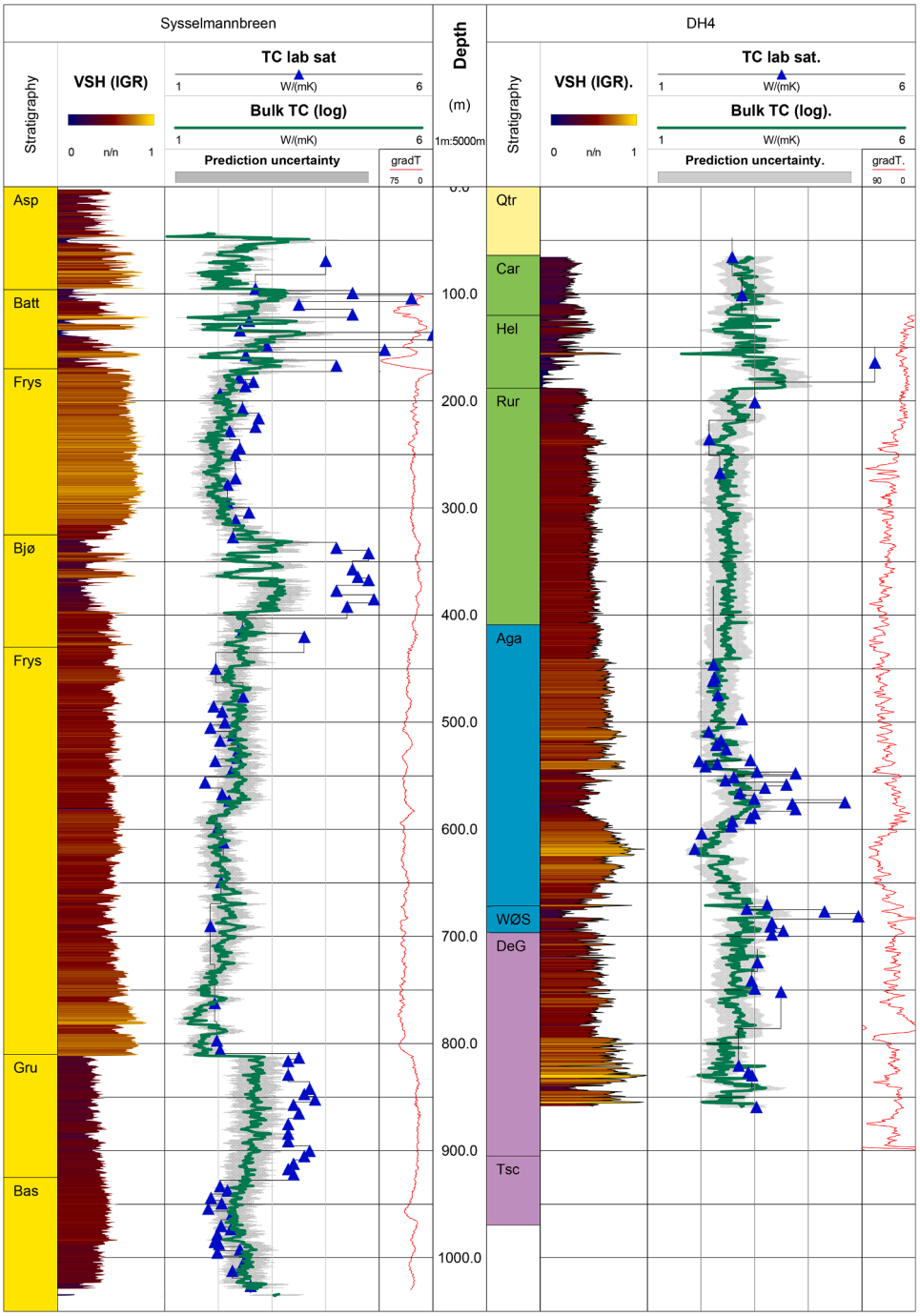

Fig. 13. Thermal conductivity estimation from wireline logs for the DH4 (A) and Sysselmannbreen (B) boreholes. The measured thermal conductivities are included for comparison.

the removal of several kilometers of overburden are likely to result in overall higher geothermal gradients (e.g., Craw et al., 1994). However, further complexity is added by the high lateral variation (i.e. dipping strata) in Svalbard's stratigraphy, the highly varying topography, the highly transient fluid flow conditions, and the influence of major fault and fracture zones distributed throughout Svalbard and its surroundings. To the west of Svalbard, the interplay between significant deposition and active sea floor spreading further complicates the present and past heat flow distribution.

On a regional scale the disequilibrium is likely even more profound, while the uplifted areas likely display enhanced geothermal gradients, the adjacent areas of rapid deposition are likely to exhibit lower geothermal gradients as is observed elsewhere in the world (e.g., Christie and Nagihara, 2016), although it should be noted that much of this deposition occurred close to the western margin where a thinner lithosphere and hotter conditions prevail.

5.4. *The subsurface thermal state of svalbard: implications and applications*

This study synthesizes the present-day subsurface thermal state of Svalbard, with obvious implications for assessing the shallow and deeper geothermal potential beneath Longyearbyen (Fig. 19). Furthermore, the regional implications of this data-driven compilation span

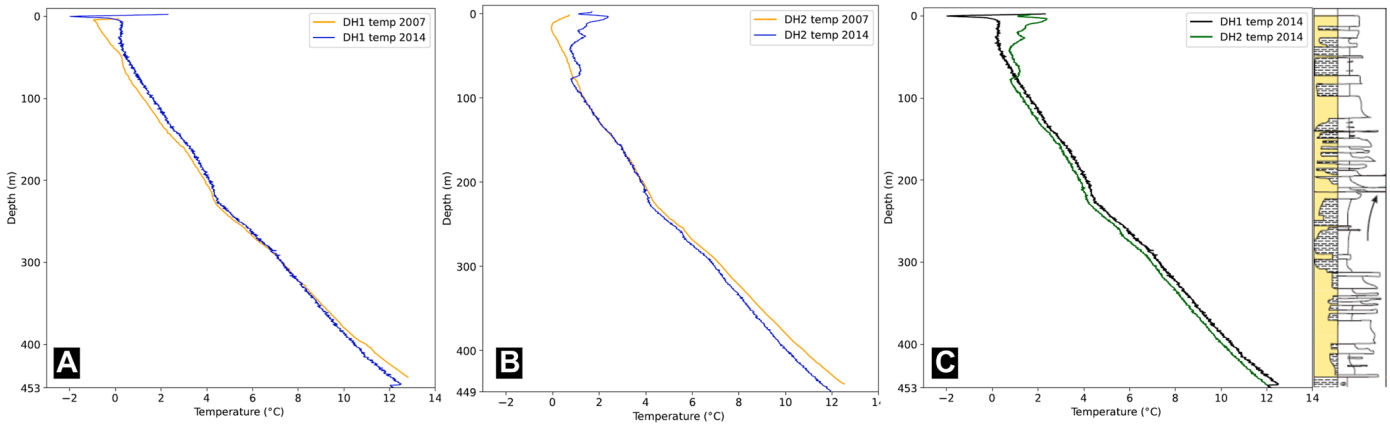

Fig. 14. Downhole temporal temperature data in DH1 and DH2 boreholes in Adventdalen. A) Downhole temperatures measured in 2007 and 2014 in DH1. C) Downhole temperatures in 2007 and 2014 in DH2. C) Temperatures measured by fibre optic cables in 2014 for DH1 and DH2. The sedimentary log is from Olaussen et al. (2019).

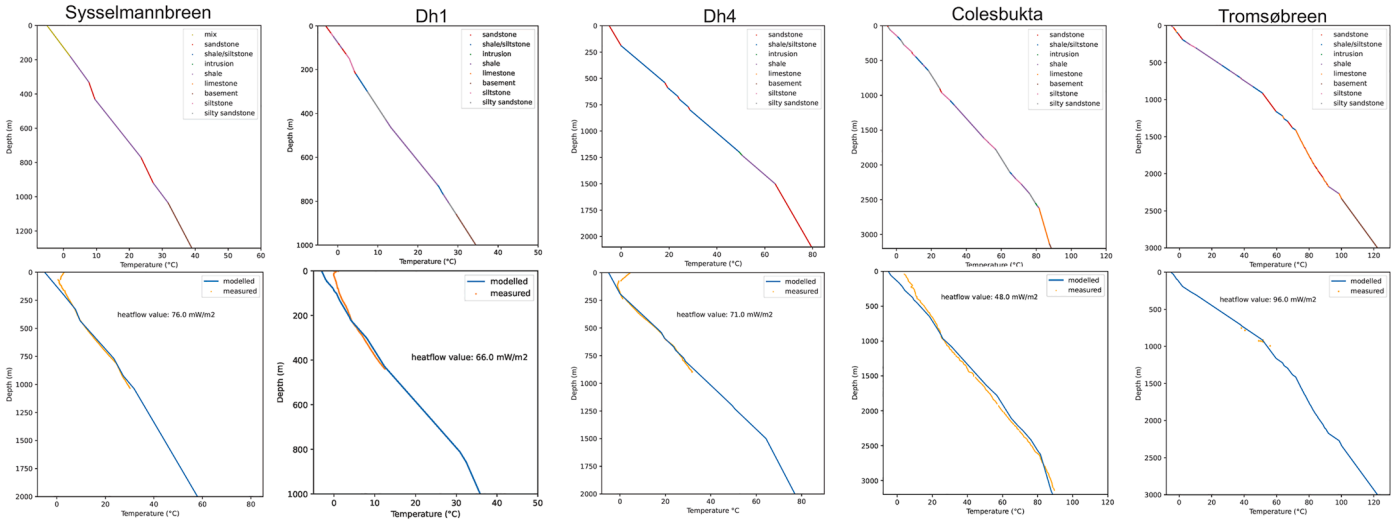

Fig. 15. 1D heatflow models of selected wells, including modelled (blue) and observed (orange) data from Sysselmannbreen, DH4, Colesbukta and Tromsøbreen. The lithologies used in the modelling are highlighted in the upper images.

from geothermal resource assessments to understanding the cryosphere development.

5.4.1. *Deep geothermal production in Longyearbyen*

As outlined above and in news articles (SNSK, 2022) deep geothermal energy is being considered as a source for heat for Svalbard's main settlement of Longyearbyen with a population of about 2400. Temperatures at the planned drilling depth of 1.5–2 km (Fig. 16), 57–79 °C, are insufficient for electricity generation but could provide heat to this Arctic community. Heat could potentially be fed into the existing district heating system (DHS), presently operating at temperatures of 120 °C on coal-fueled power.

To minimize the geological and technological risk (e.g., rock-fluid interactions, seismicity, hydrostatic vs underpressured regime, hydrocarbons, poor or non-existing reservoir, water chemistry) a closed-loop DBHE is planned, with a horizontal well component targeting the Permian spiculitic Kapp Starostin Formation predicted at 1400–1600 m depth (Fig. 16), where thermal conductivity is available only from outcrop samples (Daleng and Aftret, 2021). Use of a DBHE results in significantly lower temperatures produced than the subsurface rock temperature, something which will have to be compensated using industrial heat pumps. As a pilot project, two such wells are planned to be drilled in Longyearbyen, giving an energy yield of ca 225 kW per well or 2 GWh heat per year (ex well, without heat pump), running the system in thermal equilibrium. With 13 such wells, the base load of Longyearbyen heat consumption could be covered. The wells could be located near the existing district heating network, which in parts runs at a temperature of 120 °C. From autumn 2023 the coal-fuelled power plant will be shut down and diesel will be the prime energy source for Longyearbyen, which will result in a reduction of the district heating network temperature to 70–80 °C, fitting to the chosen geothermal heat pump system.

An ongoing research project is also evaluating the geothermal potential of a DBHE with significant horizontal components at a depth of up to five kilometers beneath Longyearbyen. For electricity generation, rock temperatures exceeding 150 °C are required for enhanced geothermal systems (Lund et al., 2008). Beneath Longyearbyen these temperatures are predicted to occur at 3.5–4.1 km based on the geothermal gradients in DH2, DH4 and DH5. Geologically these might correspond to a thick succession of Devonian sandstones or crystalline bedrock. Fractured Devonian sedimentary rocks may represent a potential geothermal reservoir but at markedly increased drilling and production costs.

5.4.2. *Shallow geothermal heat storage in Longyearbyen*

In addition to deep geothermal energy potential, renewable energy

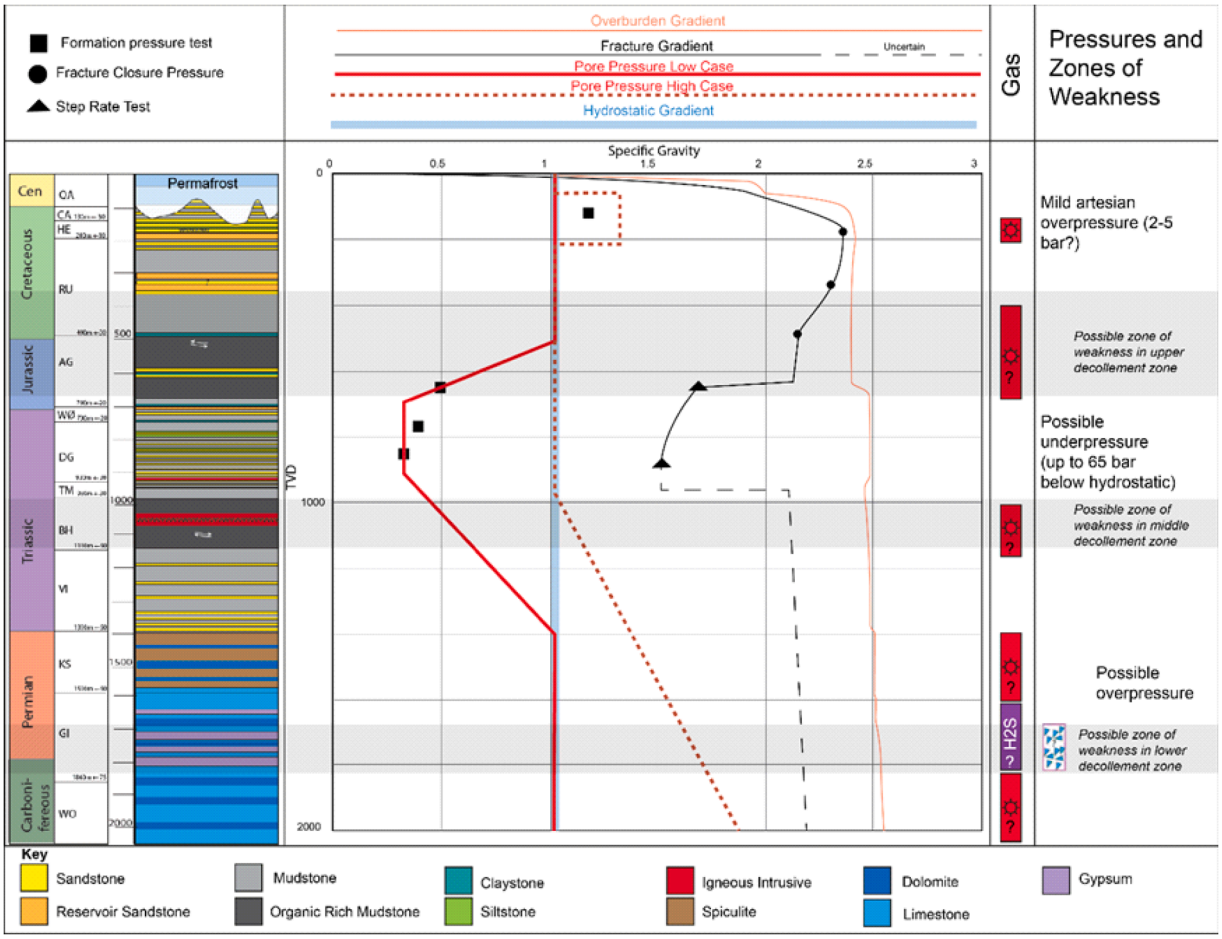

Fig. 16. Geothermal well prognosis for the Longyearbyen area. Modified from Olaussen and Birchall (2022), in SNSK (2022). Formation abbreviations from shallow to deep: QA = Quaternary, CA = Carolinefjellet, HE = Helvetiafjellet, RU = Rurikfjellet, AG = Agardhfjellet, WØ = Wilhelmøya Subgroup, DG = De Geerdalen, TM = Tschermakfjellet, BH = Botneheia, VI = Vikinghøgda, KS = Kapp Starostin, GI = Gipshuken, WO = Wordiekammen.

sources like wind and solar power may potentially feed Longyearbyen. However, these are not stable year-round energy sources and energy production will vary temporally. To optimize storing excess energy during over-production and utilizing it during periods of lower production, shallow heat storage is possible (Sommer et al., 2015; Somogyi et al., 2017).

Such storage requires establishing borehole heat exchangers in the bedrock, and their depth and amount will depend on the thermal properties and the demand of the integrated energy supply system of the town. To scale the borehole thermal energy storage (BTES) appropriately, the first should be measured in-situ, while the second would need to be modelled. In Longyearbyen, a pilot borehole was drilled near the airport at the mouth of Blomsterdalen (Figs. 19 and 20), and more are planned (Kurttila, 2021; Snoen, 2021). However, the presence of shallow gas beneath the permafrost and permeable fractured sandstone layers that may transport excess heat away from the temporary storage site significantly increases the risk.

The pilot borehole was established down to the depth of 200 m, with casing down to 12 m depth. The bedrock was encountered at 6 m depth, and the groundwater level, determined from data analysis, was estimated to be at 40 m depth. A single 40 mm U-pipe collector was inserted to 197 m depth, resulting in 157 m of the effective length of collector. A thermal response test (TRT) with added heating effect of 8 kW was carried out for 115 h. Kilfrost collector fluid ($\rho = 1195 \frac{kg}{m^3}, c_p = 3046 \frac{J}{kgK}$) with circulation flow of 30 l/min was implemented to achieve the effect. The results of TRT (Fig. 20) helped to understand the thermal properties underground affected by groundwater level and mineral distribution in the stratigraphy and showed reasonable effect in areas influenced by permafrost. The average values of thermal conductivity and resistance were found as $\lambda = 3.05 \frac{W}{mK} and R_b = 0.9 \frac{Km}{W}$ respectively (Kurttila, 2021; Snoen, 2021). The presence of the equipped borehole provides the possibility for further investigation in the area, which can be used in future projects.

Should such a BTES be installed, a matrix of the boreholes will be drilled into the rock through the permafrost. The performance of the entire system and its influence on the permafrost will need to be modelled for an accurate design. Different matrix geometries and operational scenarios, together with environmental conditions, can be modelled. A trial model for a hypothetical BTES in the area in focus was built by Jin (2020) and run for a few scenarios. The results revealed that such an approach could be used as a design tool to answer what is the temperature regime change in the volume of BTES, and what volume is affected by phase change of water content in the soil and potentially needs attention regarding the permafrost stability. The proposed scenario with a thermal insulation layer showed better performance of BTES but higher degradation of the permafrost layer, which can be addressed by introducing a thermal insulation coating around the borehole in its upper part, for example, as it was considered in geothermal heat extraction concept study in Longyearbyen (Jochmann et al., 2021). In summary, a comprehensive approach to design considering the above-mentioned aspects may lead to the scale of the BTES system, which best meets the requirements of the expected heat demand of society and its inter-seasonal need for heat storage.

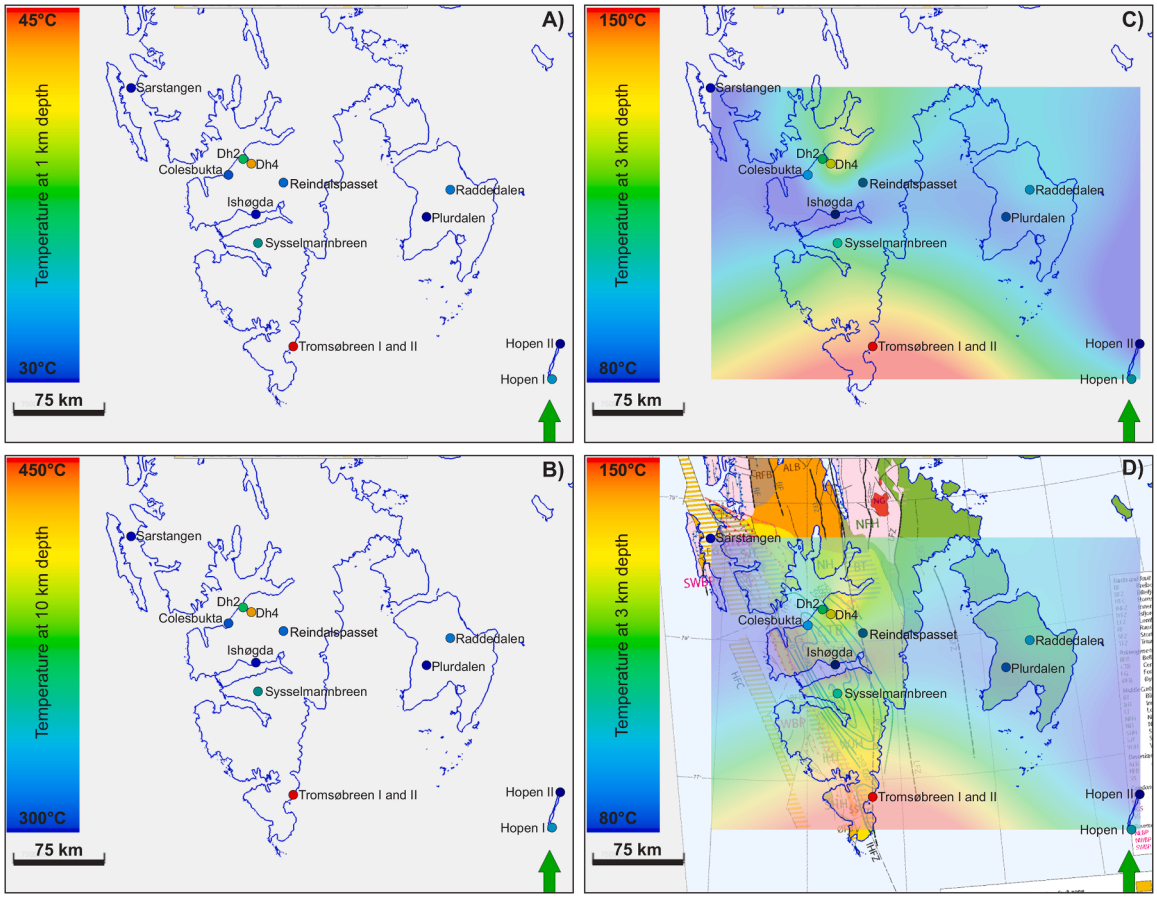

Fig. 17. Map of Svalbard from Sarstangen to Tromsøbreen with temperatures at 1 km, 3 km and 10 km, integrated with the tectonic element map. A) Temperatures in boreholes at 1 km depth, see Table 2 for details. B) Predicted temperatures in boreholes at 10 km depth. C) Combination of predicted and measured temperatures at 3 km depth, including extrapolation using convergent interpolation. D) Temperature map at 3 km depth, as in C), but also overlying the main structural elements (see Fig. 2 for details). The structural elements overlay is from Dallmann (2015).

5.4.3. *Regional and circum-Arctic implications*

Our study provides important calibration points for addressing circum-Arctic geothermal potential, but also for calibrating the permafrost thickness, onshore gas hydrate stability and source rock maturity.

In Svalbard, permafrost thickness is primarily constrained from shallow boreholes (Isaksen et al., 2000) and thermal modelling (Etzelmüller et al., 2011). The previously overlooked exploration boreholes provide important constraints on permafrost thickness and also sub-permafrost gas accumulations (Birchall et al., 2021). Gas and permafrost can under the right pressure-temperature conditions lead to the formation of gas hydrates (Betlem et al., 2019). Olaussen et al. (2023) provide a synthesis of the maturation of Mesozoic organic-rich shales, indicating a strong west-east trend from overmature in western Spitsbergen to immature in eastern Svalbard.

No geothermal potential assessment has so far been conducted for Svalbard. Lund et al. (2008) present a Nordic overview, highlighting that 55% of Iceland's primary energy production is sourced from geothermal energy and that Sweden is at the forefront of using geothermal heat pumps for space heating. Based on a series of geothermal maps of Canada (Grasby et al., 2009), Majorowicz and Grasby (2010a) provide a resource assessment for Canada, while Majorowicz and Grasby (2010b) focus on the deeper enhanced geothermal system potential. On a smaller scale, Gascuel et al. (2020) estimate the geothermal potential of Anticosti Island.

5.4.4. *Knowledge and data gaps*

The present study identifies a major data gap in terms of physical measurements of thermal conductivity in drilled strata older than the Late Triassic succession in the DH4 borehole, with the exception of the averaged values from the Colesbukta borehole on an unknown number of samples reported by (Khutorskoy et al., 2013). Only two samples from outcrops provide thermal conductivity for the Kapp Starostin Formation. Similarly, no temperature data beyond 900 m exists near Longyearbyen. As the only obvious place for geothermal production is where the infrastructure and roads are near Longyearbyen, limited geophysical surveying was conducted, with the notable exception of the regional MT surveys of Beka (2016). High-resolution gravity and magnetic data, as conducted by Peng et al. (2019) in northeastern China, could constrain the geothermal targets. Similarly, acquisition of seismic reflection data coupled with seismic inversion constrained by well data can be used to predict lithofacies and porosity (Feng et al., 2020).

Large uncertainty still exists related to what controls the strong lateral variation in heat flow across Svalbard and to what extent the paleosurface temperatures influenced the recorded heat flow. Both present-day and past thermal regimes seem closely linked to the geological evolution and structural architecture of Svalbard. Data-driven crustal scale thermal modelling, as conducted across southern Svalbard by Grad and Majorowicz (2020), is required across areas of the deep boreholes to couple deep and shallow processes related to the thermal field. Once confidence is gained along data-driven profiles including both thermal and geological information, a natural progression would involve the construction of a 3D geothermal model as conducted for Denmark (Balling et al., 2022; Fuchs et al., 2020).

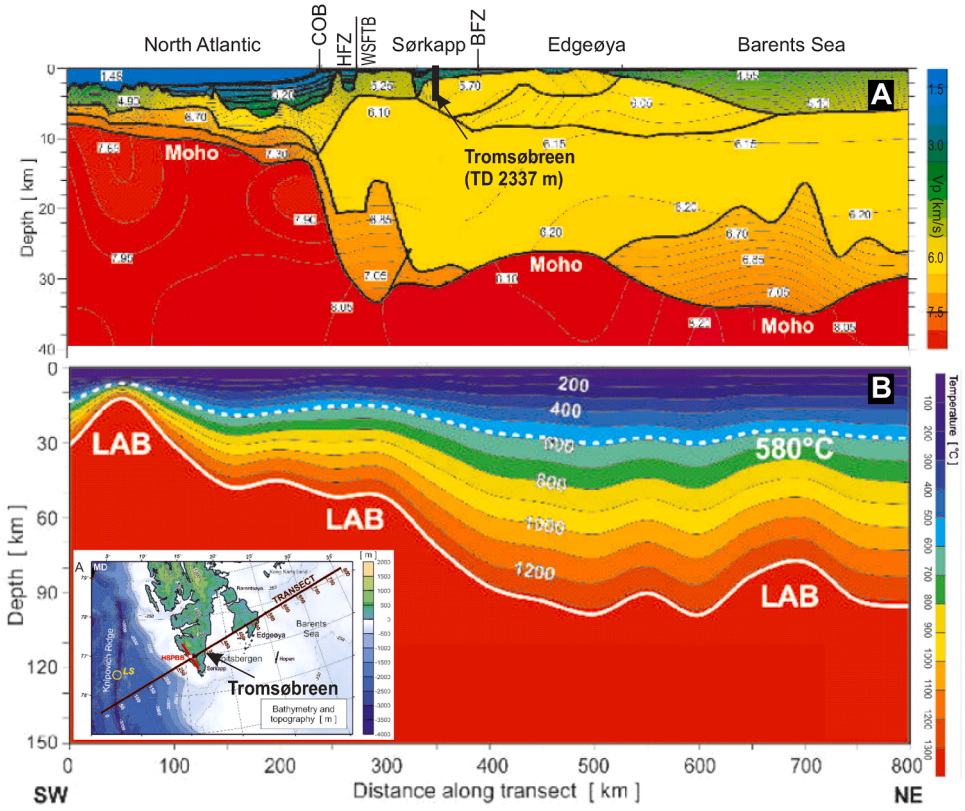

Fig. 18. Crustal structure and thermal profile across the regional HORSTED transect, highlighting the position of the anomalous Tromsøbreen borehole. Figures adapted from Grad and Majorowicz (2020).

Fig. 19. Map of near town area with temperature gradients from shallow and deep boreholes and the potential deep geothermal drill site. The base satellite imagery is from Norwegian Polar Institute (2014).

6. Conclusions

In this contribution we have synthesized previously unpublished thermal conductivity and borehole temperature data from four research boreholes with borehole temperatures from ten petroleum exploration boreholes to provide an estimate of the subsurface thermal state of Svalbard. We have focused on integrating the subsurface data with the geological evolution to understand the spatial variability in thermal regime and with implications for the deep geothermal energy potential near Longyearbyen. Our main findings may be summarized as follows:

- Deep (>200 m) boreholes onshore Svalbard, covering depths from 500 to 3304 m, offer an average geothermal gradient of 33 °C/km, ranging from 24 °C/km to 55 °C/km
- The increased regional geothermal gradient onshore Svalbard is likely related to a thinner lithosphere. Locally enhanced heat flow is related to major fault zones and areas affected by recent volcanism.
- Thermal conductivity analysis of 232 samples from Mesozoic-Cenozoic shales and sandstones cored by research wells indicate average thermal conductivity of 3.92 W/m K for sandstones and 2.31 W/m K for shales.
- Geothermal gradients of 43 °C/km are recorded in the uppermost 1 km beneath Longyearbyen, Svalbard's main settlement, suggesting that geothermal energy may be a viable part of Longyearbyen's energy mix in the future. A well prognosis for a hypothetical 2 km deep geothermal borehole in Longyearbyen is presented.
- The largest data gaps reflect the lack of thermal conductivity measurements on Middle Triassic and older strata, where only outcrop and averaged measurements from the Colesbukta well are available.

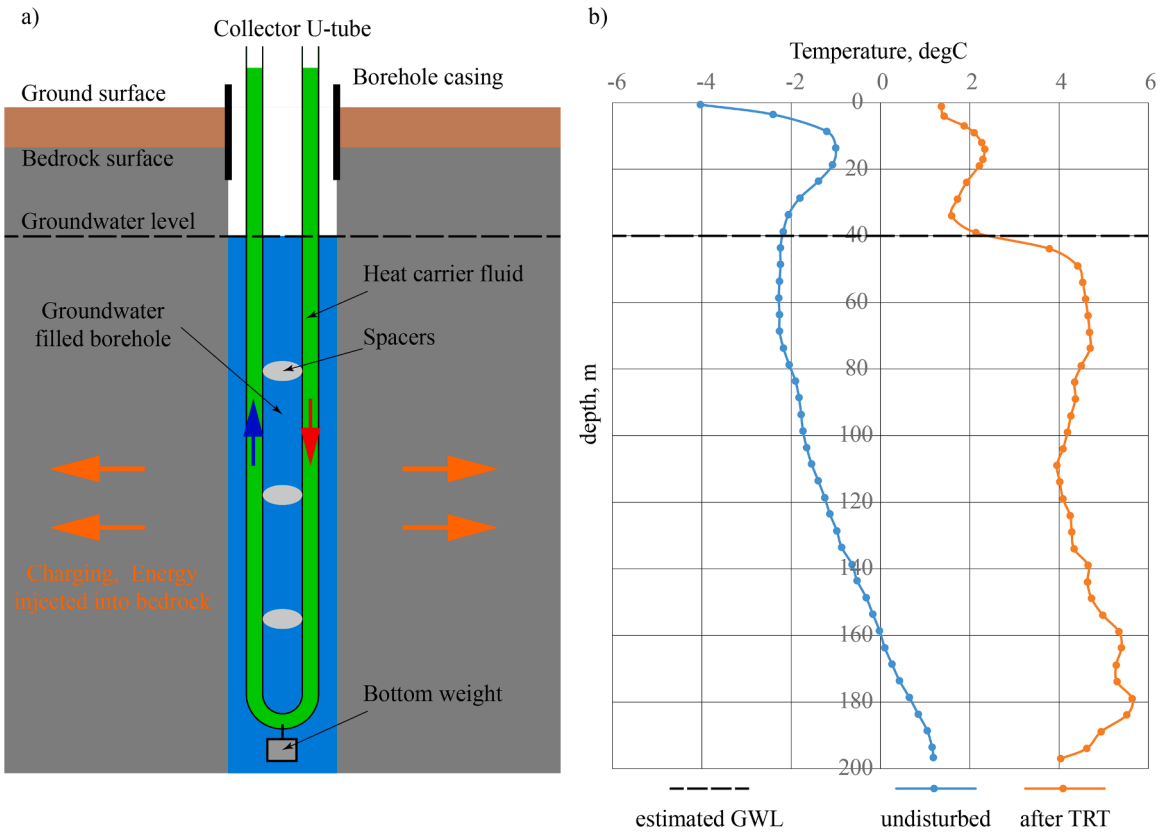

Fig. 20. Cartoon illustrating the BTES system drilled at Blomsterdalen where a thermal response test was carried out. The temperatures before and after this test are shown.

- Furthermore, good quality heat flow data from deep boreholes are required to reliably estimate heat flow density and derive temperature variation in the geologic past (i.e. paleoclimatic effects). Fully cored deep (> 1–2 km) research wells would likely be required as the existing deep petroleum exploration boreholes lack both drill cores and high-resolution temperature data.

Data availability

Borehole data used include data from the Longyearbyen CO_2 lab (Olaussen et al., 2019), the Sysselmannbreen borehole, the archive of Norsk Polar Navigasjon AS (Senger et al., 2022) and the Norwegian Petroleum Directorate, all of which are integrated at UNIS. All plotted data are available in the supplementary material.

CRediT authorship contribution statement

Kim Senger: Conceptualization, Writing – original draft, Project administration, Funding acquisition, Visualization. **Matthijs Nuus:** Formal analysis, Data curation, Visualization. **Niels Balling:** Formal analysis, Investigation, Writing – review & editing. **Peter Betlem:** Formal analysis, Data curation, Writing – review & editing. **Tom Birchall:** Writing – original draft, Visualization, Writing – review & editing. **Hanne H. Christiansen:** Data curation, Formal analysis, Writing – review & editing, Funding acquisition. **Harald Elvebakk:** Formal analysis, Investigation, Writing – review & editing. **Sven Fuchs:** Formal analysis, Writing – review & editing, Visualization. **Malte Jochmann:** Data curation, Writing – review & editing, Funding acquisition. **Peter Klitzke:** Formal analysis, Data curation, Writing – review & editing. **Kirsti Midttømme:** Writing – review & editing. **Snorre Olaussen:** Writing – original draft, Funding acquisition. **Christophe Pascal:** Formal analysis, Investigation, Data curation, Writing – review & editing. **Nil Rodes:** Visualization, Writing – review & editing. **Aleksey Shestov:** Visualization, Writing – review & editing. **Aleksandra Smyrak-Sikora:** Writing – review & editing. **Peter James Thomas:** Investigation, Writing – review & editing.

Declaration of Competing Interest

The authors confirm that they have no known competing financial or personal interests that could have influenced the work on this publication.

Acknowledgements

The presented synthesis effort received funding from both the Norwegian Research Council (projects Environmentally friendly energy for Svalbard – utilization of geothermal energy/235762, UNIS CO2 lab, ARCEx/228107, NCCS/257579, FME-SUCCESS/193825, Svalbard Rock Vault/295781, Geothermal Energy – Horizontal Closed Loop System/332149) and the private sector. The geothermos project was run as a cooperation between NTNU, Asplan Viak, UNIS and SNSK. The ongoing DBHE project is led by Reelwell with partners SNSK, Halliburton, TotalEnergies, OMV and Institute for Energy Technology. We sincerely appreciate technical discussions and data provision from Willy Fjeldskaar at Tectonor and Niels Bo Nielsen at Aarhus University. Sebastian Faulkner at the UNIS library was instrumental to gain access to much of the Russian literature. Finally, we sincerely appreciate the constructive feedback from Yuriy P. Maystrenko and an anonymous reviewer and the excellent editorial handling by Christopher Bromley.

Supplementary materials

Supplementary material associated with this article can be found, in

the online version, at doi:10.1016/j.geothermics.2023.102702.

References

Albert, K., Schulze, M., Franz, C., Koenigsdorff, R., Zosseder, K., 2017. Thermal conductivity estimation model considering the effect of water saturation explaining the heterogeneity of rock thermal conductivity. Geothermics 66, 1–12. https://doi.org/10.1016/j.geothermics.2016.11.006.

Alimonti, C., Conti, P., Soldo, E., 2021. Producing geothermal energy with a deep borehole heat exchanger: exergy optimization of different applications and preliminary design criteria. Energy 220, 119679. https://doi.org/10.1016/j.energy.2020.119679.

Amundsen, H., Griffin, W., O'reilly, S.Y., 1987. The lower crust and upper mantle beneath northwestern Spitsbergen: evidence from xenoliths and geophysics. Tectonophysics 139 (3–4), 169–185.

Anell, I., Braathen, A., Olaussen, S., 2014. The Triassic-Early Jurassic of the northern Barents Shelf: a regional understanding of the Longyearbyen CO_2 reservoir. Norw. J. Geol. 94 (2–3), 83–98. http://urn.nb.no/URN:NBN:no-64623.

Antonovskaya, G.N., Basakina, I.M., Konechnaya, Y.V., 2018. Distribution of seismicity and heat flow anomalies in the barents sea region. Geotectonics 52 (1), 45–55. https://doi.org/10.1134/S001685211801003X.

Axelsson, G., Björnsson, G., Quijano, J.E., 2005. Reliability of lumped parameter modeling of pressure changes in geothermal reservoirs. In: Proceedings World Geothermal Congress. Antalya, Turkey, pp. 1–8, 24-29 April 2005.

Balling, N., Fuchs, S., Mathiesen, A., 2022. A 3D geothermal model for Denmark: temperature and resource assessment. In: Proceedings European Geothermal Congress 2022. Berlin, Germany, p. 7, 17-21 October 2022.

Banks, D., Siewers, U., Sletten, R., Haldorsen, S., Dale, B., Heim, M. and Swensen, B., 1997. The thermal springs of bockfjord, Svalbard-Hydrogeochemical Data Report, Geological Survey of Norway, Trondheim, Trondheim, Norway.

Beka, T.I., 2016. Geoelectrical Structures Beneath Spitsbergen-Svalbard derived from Magnetotelluric Imaging. University of Tromsø - the Arctic University of Norway.

Beka, T.I., Bergh, S.G., Smirnov, M., Birkelund, Y., 2017a. Magnetotelluric Signatures of the Complex Tertiary Fold–Thrust Belt and Extensional Fault Architecture Beneath Brøggerhalvøya, Svalbard, 36. Polar Research, 1409586. https://doi.org/10.1080/17518369.2017.1409586.

Beka, T.I., Senger, K., Autio, U.A., Smirnov, M., Birkelund, Y., 2017b. Integrated electromagnetic data investigation of a Mesozoic CO2 storage target reservoir-cap-rock succession. Svalbard. Journal of Applied Geophysics 136, 417–430. https://doi.org/10.1016/j.jappgeo.2016.11.021.

Beka, T.I., Smirnov, M., Bergh, S.G., Birkelund, Y., 2015. The first magnetotelluric image of the lithospheric-scale geological architecture in central Svalbard. Arctic Norway. Polar Res. 34, 26766. https://doi.org/10.3402/polar.v34.26766.

Beka, T.I., Smirnov, M., Birkelund, Y., Senger, K., Bergh, S.G., 2016. Analysis and 3D inversion of magnetotelluric crooked profile data from central Svalbard for geothermal application. Tectonophysics. https://doi.org/10.1016/j.tecto.2016.07.024.

Betlem, P., Midttømme, K., Jochmann, M., Senger, K., Olaussen, S., 2018. Geothermal Gradients on Svalbard, Arctic Norway, First EAGE/IGA/DGMK Joint Workshop on Deep Geothermal Energy. Europ. Assoc. Geoscient. Engin., Strasbourg. https://doi.org/10.3997/2214-4609.201802945. Nov 2018cp-577-00017.

Betlem, P., Roy, S., Birchall, T., Hodson, A., Noormets, R., Römer, M., Skogseth, R., Senger, K., 2021. Modelling of the gas hydrate potential in Svalbard's fjords. J. Nat. Gas Sci. Eng. 94, 104127 https://doi.org/10.1016/j.jngse.2021.104127.

Betlem, P., Senger, K., Hodson, A., 2019. 3D thermo-baric modelling of the gas hydrate stability zone onshore central Spitsbergen. Arctic Norway. Marine Petrol. Geol. 100, 246–262. https://doi.org/10.1016/j.marpetgeo.2018.10.050.

Birchall, T., Jochmann, M., Betlem, P., Senger, K., Hodson, A., Olaussen, S., 2021. Permafrost trapped natural gas in svalbard, Norway. Cryosphere Discuss. 1–47. https://doi.org/10.5194/tc-2021-226.

Birchall, T., Senger, K., Hornum, M.T., Olaussen, S., Braathen, A., 2020. Underpressure in the northern Barents shelf: causes and implications for hydrocarbon exploration. Am. Assoc. Pet. Geol. Bull. 104 (11), 2267–2295. https://doi.org/10.1306/02272019146.

Blackwell, J., 1954. A transient-flow method for determination of thermal constants of insulating materials in bulk part I—theory. J. Appl. Phys. 25 (2), 137–144. https://doi.org/10.1063/1.1721592.

Bording, T.S., Nielsen, S.B., Balling, N., 2019. Determination of thermal properties of materials by monte carlo inversion of pulsed needle probe data. Int. J. Heat Mass Transf. 133, 154–165. https://doi.org/10.1016/j.ijheatmasstransfer.2018.12.104.

Braathen, A., Bælum, K., Christiansen, H.H., Dahl, T., Eiken, O., Elvebakk, H., Hansen, F., Hanssen, T.H., Jochmann, M., Johansen, T.A., Johnsen, H., Larsen, L., Lie, T., Mertes, J., Mørk, A., Mørk, M.B., Nemec, W.J., Olaussen, S., Oye, V., Rød, K., Titlestad, G.O., Tveranger, J., Vagle, K., 2012. Longyearbyen CO_2 lab of Svalbard, Norway – first assessment of the sedimentary succession for CO_2 storage. Norw. J. Geol. 92 (4), 353–376. https://njg.geologi.no/vol-91-100/details/1/63-63.html.

Brekke, T., Krajewski, K.P., Hubred, J.H., 2014. Organic geochemistry and petrography of thermally altered sections of the Middle Triassic Botneheia Formation on south-western Edgeøya, Svalbard. Norwegian Petrol. Directorate Bull. 11, 111–128. https://www.npd.no/globalassets/1-npd/publikasjoner/npd-bulletins/npd-bulletin-11-2015.pdf.

Chen, Z., Grasby, S.E., Dewing, K., Osadetz, K.G., Brent, T., 2018. Geological controls on the present temperature field of the western Sverdrup Basin, Canadian Arctic Archipelago. Basin Res. 30, 479–496. https://doi.org/10.1111/bre.12232.

Christiansen, H., 2009. LF-B-1 Lunckefjell (20-2009), Global terrestrial network for permafrost - database, http://gtnpdatabase.org/boreholes/view/66.

Christiansen, H.H., Etzelmüller, B., Isaksen, K., Juliussen, H., Farbrot, H., Humlum, O., Johansson, M., Ingeman-Nielsen, T., Kristensen, L., Hjort, J., Holmlund, P., Sannel, A.B.K., Sigsgaard, C., Åkerman, H.J., Foged, N., Blikra, L.H., Pernosky, M.A., Ødegård, R.S., 2010. The thermal state of permafrost in the nordic area during the international polar year 2007–2009. Permafr Periglac Process 21 (2), 156–181. https://doi.org/10.1002/ppp.687.

Christiansen, H.H., Gilbert, G.L., Neumann, U., Demidov, N., Guglielmin, M., Isaksen, K., Osuch, M. and Boike, J., 2021. Ground ice content, drilling methods and equipment and permafrost dynamics in Svalbard 2016–2019 (PermaSval). SESS report 2020-The State of Environmental Science in Svalbard-an annual report, 3 10.5281/zenodo.4294095.

Christie, C.H., Nagihara, S., 2016. Geothermal gradients of the northern continental shelf of the Gulf of Mexico. Geosphere 12 (1), 26–34. https://doi.org/10.1130/GES01163.1.

Ciriaco, A.E., Zarrouk, S.J., Zakeri, G., 2020. Geothermal resource and reserve assessment methodology: overview, analysis and future directions. Renew. Sustain. Energy Rev. 119, 109515 https://doi.org/10.1016/j.rser.2019.109515.

Colgan, W., Wansing, A., 2021. Greenland geothermal heat flow database and map. GEUS Dataverse. https://doi.org/10.22008/FK2/F9P03L.

Colgan, W., Wansing, A., Mankoff, K., Lösing, M., Hopper, J., Louden, K., Ebbing, J., Christiansen, F.G., Ingeman-Nielsen, T., Liljedahl, L.C., 2022. Greenland geothermal heat flow database and map (version 1). Earth Syst. Sci. Data 14 (5), 2209–2238. https://doi.org/10.5194/essd-14-2209-2022.

Corfu, F., Polteau, S., Planke, S., Faleide, J.I., Svensen, H., Zayoncheck, A., Stolbov, N., 2013. U–Pb geochronology of Cretaceous magmatism on Svalbard and Franz Josef Land, Barents Sea large igneous province. Geol. Mag. 150 (6), 1127–1135. https://doi.org/10.1017/S0016756813000162.

Crane, K., Eldholm, O., Myhre, A.M., Sundvor, E., 1982. Thermal implications for the evolution of the Spitsbergen transform fault. Tectonophysics 89 (1–3), 1–32. https://doi.org/10.1016/0040-1951(82)90032-4.

Crane, K., Sundvor, E., Buck, R., Martinez, F., 1991. Rifting in the northern Norwegian-Greenland Sea: thermal tests of asymmetric spreading. J Geophys Res 96 (B9), 14529–14550. https://doi.org/10.1029/91JB01231.

Crane, K., Sundvor, E., Foucher, J.-P., Hobart, M., Myhre, A., LeDouaran, S., 1988. Thermal evolution of the western Svalbard margin. Mar. Geophys. Res. 9 (2), 165–194.

Craw, D., Koons, P.O., Winslow, D., Chamberlain, C.P., Zeitler, P., 1994. Boiling fluids in a region of rapid uplift, Nanga Parbat Massif, Pakistan. Earth Planet. Sci. Lett. 128 (3), 169–182. https://doi.org/10.1016/0012-821X(94)90143-0.

Daleng, V.M., Aftret, H.M., 2021. Suitability of Thermosyphon as a Ground Freezing Technology in Longyearbyen. NTNU, Trondheim.

Dallmann, W., 2015. Geoscience Atlas of Svalbard. Norsk Polarinstitutt Rapportserie 148, 292. http://hdl.handle.net/11250/2580810.

Dallmann, W.K., Dypvik, H., Gjelberg, J.G., Harland, W.B., Johannessen, E.P., Keilen, H. B., Larssen, G.B., Lønøy, A., Midbøe, P.S., Mørk, A., Nagy, J., Nilsson, I., Nøttvedt, A., Olaussen, S., Pcelina, T.M., Steel, R.J., Worsley, D., 1999. Lithostratigraphic Lexicon of Svalbard: Review and Recommendations For Nomenclature Use. Norsk Polarinstitutt, Tromsø, p. 318.

Dumais, M.A., Gernigon, L., Olesen, O., Lim, A., Johansen, S., Brönner, M., 2022. Crustal and Thermal Heterogeneities across the Fram Strait and the Svalbard Margin. Tectonics 41 (10). https://doi.org/10.1029/2022TC007302 e2022TC007302.

Elvebakk, H., 2008. Results of Borehole Logging in CO2 wells, Dh1-CO2-07 and Dh2-CO2-07. NGU Report, Longyearbyen, Svalbard.

Elvebakk, H., 2010. Results of borehole logging in well LYB CO2, Dh4 of 2009, Longyearbyen, Svalbard, NGU, Trondheim, Norway.

Elvebakk, H., Rønning, J., Jochman, M., Henningsen, T., Johannessen, E., Bering, D., Elvebakk, G., 2008. Geophysical Borehole Logging in Dh 10-2008 At Sysselmannbreen. Svalbard, Geological Survey of Norway, Trondheim, Norway.

Etzelmüller, B., Schuler, T.V., Isaksen, K., Christiansen, H.H., Farbrot, H., Benestad, R., 2011. Modeling the temperature evolution of Svalbard permafrost during the 20th and 21st century. The Cryosphere 5 (1), 67–79. https://doi.org/10.5194/tc-5-67-2011.

Faleide, J.I., Tsikalas, F., Breivik, A.J., Mjelde, R., Ritzmann, O., Engen, Ø., Wilson, J., Eldholm, O., 2008. Structure and evolution of the continental margin off Norway and the Barents Sea. Episodes J. Int. Geosci. 31 (1), 82–91. https://doi.org/10.18814/epiiugs/2008/v31i1/012.

Feng, R., Balling, N., Grana, D., 2020. Lithofacies classification of a geothermal reservoir in Denmark and its facies-dependent porosity estimation from seismic inversion. Geothermics 87, 101854. https://doi.org/10.1016/j.geothermics.2020.101854.

Fiedler, A., Faleide, J.I., 1996. Cenozoic sedimentation along the southwestern Barents Sea margin in relation to uplift and erosion of the shelf. Glob. Planet Change 12 (1), 75–93. https://doi.org/10.1016/0921-8181(95)00013-5.

Fuchs, S., Balling, N., Förster, A., 2015. Calculation of thermal conductivity, thermal diffusivity and specific heat capacity of sedimentary rocks using petrophysical well logs. Geophys. J. Int. 203 (3), 1977–2000. https://doi.org/10.1093/gji/ggv403.

Fuchs, S., Balling, N., Mathiesen, A., 2020. Deep basin temperature and heat-flow field in Denmark–New insights from borehole analysis and 3D geothermal modelling. Geothermics 83, 101722. https://doi.org/10.1016/j.geothermics.2019.101722.

Fuchs, S., Norden, B., Artemieva, I., Chiozzi, P., Dedecek, P., Demezhko, D., Förster, A., Gola, G., Gosnold, W., Hamza, V., Harris, R., He, L., Huang, S., Kohl, T., Lee, Y., Liu, S., Podugu, N., Negrete-Aranda, R., Poort, J., Roy, S., Tanaka, A., Vakhitova, G., Verdoya, M., Commission, I.H.F., 2021. The global heat flow database: Release 2021, https://doi.org/10.5880/fidgeo.2021.014.

Gac, S., Minakov, A., Shephard, G.E., Faleide, J.I., Planke, S., 2020. Deformation analysis in the Barents Sea in relation to Paleogene transpression along the Greenland-Eurasia plate boundary. Tectonics 39 (10). https://doi.org/10.1029/2020TC006172 e2020TC006172.

Ganguly, N., Spence, G.D., Chapman, N.R., Hyndman, R.D., 2000. Heat flow variations from bottom simulating reflectors on the Cascadia margin. Mar. Geol. 164 (1), 53–68. https://doi.org/10.1016/S0025-3227(99)00126-7.

Gascuel, V., Bédard, K., Comeau, F.-A., Raymond, J., Malo, M., 2020. Geothermal resource assessment of remote sedimentary basins with sparse data: lessons learned from Anticosti Island. Canada. Geothermal Energy 8 (1), 1–32. https://doi.org/10.1186/s40517-020-0156-1.

Geissler, W.H., Estrada, S., Riefstahl, F., O'Connor, J.M., Spiegel, C., Van den Boogard, P. and Klügel, A., 2019. Middle Miocene magmatic activity in the Sophia Basin, Arctic Ocean—evidence from dredged basalt at the flanks of Mosby Seamount. arktos, 5(1): 31–48 https://doi.org/10.1007/s41063-019-00066-8.

Gjelberg, J., Steel, R., 1981. An outline of Lower-Middle Carboniferous sedimentation on Svalbard: effects of tectonic, climatic and sea level changes in rift basin sequences. Geol. North Atlantic Borderlands 543–561. https://archives.datapages.com/data/cspg_sp/data/007/007001/543_cspgsp0070543.htm.

Gjelsvik, 1963. Remarks On the Structure and Composition of the Sverrefjellet volcano, Bockfjorden, Vestspitsbergen, 1962. Norsk Polarinstitutt Årbok, pp. 50–54.

Grad, M., Majorowicz, J., 2020. Geophysical Properties of the Crust and Upper Mantle of the Ocean-Continent Transition in Svalbard area. Polish Polar Research, pp. 1–22. https://doi.org/10.24425/ppr.2020.132567.

Grasby, S., Majorowicz, J., Ko, M., 2009. Geothermal Maps of Canada. G.S.o.C.O.F. 6167, Ottawa, Canada. Editor.

Griffin, W., Nikolic, N., O'Reilly, S.Y., Pearson, N., 2012. Coupling, decoupling and metasomatism: evolution of crust–mantle relationships beneath NW Spitsbergen. Lithos 149, 115–135. https://doi.org/10.1016/j.lithos.2012.03.003.

Grundvåg, S.A., Johannessen, E.P., Helland-Hansen, W., Plink-Björklund, P., 2014. Depositional architecture and evolution of progradationally stacked lobe complexes in the Eocene Central Basin of Spitsbergen. Sedimentology 61 (2), 535–569. https://doi.org/10.1111/sed.12067.

Guyer, J.E., Wheeler, D., Warren, J.A., 2009. FiPy: partial differential equations with Python. Comput. Sci. Eng. 11 (3), 6–15. https://doi.org/10.1109/MCSE.2009.52.

Hacıoğlu, Ö., Başokur, A.T., Diner, Ç., 2021. Geothermal potential of the eastern end of the Gediz basin, western Anatolia, Turkey revealed by three-dimensional inversion of magnetotelluric data. Geothermics 91, 102040. https://doi.org/10.1016/j.geothermics.2020.102040.

Haldorsen, S., Heim, M., 1999. An Arctic groundwater system and its dependence upon climatic change: an example from Svalbard. Permafr Periglac Process 10 (2), 137–149. https://doi.org/10.1002/(SICI)1099-1530(199904/06)10:2<137::AID-PPP316>3.0.CO;2-%23.

Harrison, W.E., Luza, K.V., Prater, M.L., Cheung, P.K., Ruscetta, C., 1982. Geothermal resource assessment in Oklahoma. In: Geothermal energy exploration and resource assessment technical conference. Salt Lake City, UT, USA, 5 Apr 1982. https://www.osti.gov/biblio/7369499.

Helland-Hansen, W., Grundvåg, S.A., 2021. The Svalbard Eocene-Oligocene (?) Central Basin succession: sedimentation patterns and controls. Basin Res. 33 (1), 729–753. https://doi.org/10.1111/bre.12492.

Henne, I., Kocbach, J. and Hauge, R., 2014. Thermal modelling of the subsurface in Adventdalen and Sysselmannbreen at Svalbard using COMSOL Multiphysics.

Henriksen, E., Bjørnseth, H.M., Hals, T.K., Heide, T., Kiryukhina, T., Kløvjan, O.S., Larssen, G.B., Ryseth, A.E., Rønning, K., Sollid, K., Stoupakova, A., Spencer, A.M., Embry, A.F., Gautier, D.L., Stoupakova, A.V., Sørensen, K., 2011. Uplift and erosion of the greater Barents Sea: impact on prospectivity and petroleum systems. Arctic Petrol. Geol. https://doi.org/10.1144/m35.17, 0.

Hubred, J.H., 2006. Unpublished MSc Thesis. University of Oslo, Oslo, p. 303.

Humlum, O., 2005. Holocene permafrost aggradation in Svalbard. Geolog. Society 242 (1), 119–129, 10.1144./GSL.SP.2005.242.01.11.

Isaksen, K., Holmlund, P., Sollid, J.L., Harris, C., 2001. Three deep alpine-permafrost boreholes in Svalbard and Scandinavia. Permafr Periglac Process 12 (1), 13–25. https://doi.org/10.1016/0040-1951(87)90095-3.

Isaksen, K., Mühll, D.V., Gubler, H., Kohl, T., Sollid, J.L., 2000. Ground surface-temperature reconstruction based on data from a deep borehole in permafrost at Janssonhaugen. Svalbard. Annals Glaciol. 31 (1), 287–294. https://doi.org/10.3189/172756400781820291.

Iversen, J., 2013. Geothermal Energy and District Heating. University of Tromsø - the Arctic University of Norway, Ny-Ålesund, Svalbard, p. 101.

Jamtveit, B., Hammer, Ø., Andersson, C., Dysthe, D., Heldmann, J., Fogel, M.L., 2006. Travertines from the Troll thermal springs, Svalbard. Norwegian Journal of Geology/Norsk Geologisk Forening 86 (4).

Jessop, A.M., Ghomshei, M.M., Drury, M.J., 1991. Geothermal energy in Canada. Geothermics 20 (5–6), 369–385. https://doi.org/10.1016/0375-6505(91)90027-S.

Jin, X., 2020. Heat storage in rock and soil in permafrost conditions.

Jochmann, M., Aalberg, A., Christiansen, H., Musæus, T.E., Nygård, G., Moen, J.I., Olaussen, S., Ropphaugen, G.O., Sellevold, M.O.D., Shestov, A., Talstad, S., Theloy, T., November 2021. Geothermal heat extraction in Longyearbyen - an applied concept study. In: Poster at the Svalbard Science Conference 2021. Oslo. https://doi.org/10.13140/RG.2.2.34398.97607.

Johannessen, E.P., Henningsen, T., Bakke, N.E., Johansen, T.A., Ruud, B.O., Riste, P., Elvebakk, H., Jochmann, M., Elvebakk, G., Woldengen, M.S., 2011. Palaeogene clinoform succession on Svalbard expressed in outcrops, seismic data, logs and cores. First Break 29, 35–44. https://doi.org/10.3997/1365-2397.2011004.

Jones, F., Majorowicz, J., Embry, A., Jessop, A., 1990. Geothermal gradients and terrestrial heat flow along a south-north profile in the Sverdrup Basin, Canadian Arctic Archipelago. Geophysics 55 (8), 1105–1107. https://doi.org/10.1190/1.1442923.

Jones, F.W., Majorowicz, J., Embry, A., 1989. A heat flow profile across the Sverdrup Basin, Canadian Arctic Islands. Geophysics 54 (2), 171–180. https://doi.org/10.1190/1.1442641.

Joshua, E.O., Ehinola, O.A., Akpanowo, M.A., Oyebanjo, O.A., 2008. Radiogenic heat production in crustal rock samples of Southeastern Nigeria. Eur. J. Appl. Eng. Sci. Res. 23 (2), 305–316.

Kalskin Ramstad, R., de Beer, H., Midttømme, K., Koziel, J. and Willemoes-Wissing, B., 2008. Status of thermal diffusivity equipment–method development 2005-2008. NGU Report.

Khutorskoi, M., Leonov, Y.G., Ermakov, A., Akhmedzyanov, V., 2009. Abnormal heat flow and the trough's nature in the Northern Svalbard plate. Dokl. Earth Sci. 29.

Khutorskoi, M.D., Antonovskaya, G.N., Basakina, I.M., Teveleva, E.A., 2022. Seismicity and Heat Flow along the Periphery of the East European Platform. J. Volcanol. Seismolog. 16 (2), 150–167. https://doi.org/10.1134/S074204632202004X.

Khutorskoy, M., Akhmedzianov, V., 2008. Geothermal field of svalbard plate northern part: problems and evaluations. RUDN J. Ecol. Life Safety (3), 49–58. https://journals.rudn.ru/ecology/article/view/12643.

Khutorskoy, M.D., Akhmedzyanov, V.R., Ermakov, A.V., Leonov, Y.G., Podgornykh, L.V., Polyak, B.G., Sukhikh, E.A., Tsybulya, L.A., 2013. Geothermics of the Arctic seas. Transactions of the Geological Institute, Moscow, Russia, p. 265.

Kierulf, H.P., Kohler, J., Boy, J.-P., Geyman, E.C., Mémin, A., Omang, O.C., Steffen, H., Steffen, R., 2022. Time-varying uplift in Svalbard—An effect of glacial changes. Geophys. J. Int. 231 (3), 1518–1534.

Klitzke, P., Sippel, J., Faleide, J.I., Scheck-Wenderoth, M., 2016. A 3D gravity and thermal model for the Barents Sea and Kara Sea. Tectonophysics 684, 131–147. https://doi.org/10.1016/j.tecto.2016.04.033.

Knies, J., Matthiessen, J., Vogt, C., Laberg, J.S., Hjelstuen, B.O., Smelror, M., Larsen, E., Andreassen, K., Eidvin, T., Vorren, T.O., 2009. The Plio-Pleistocene glaciation of the Barents Sea–Svalbard region: a new model based on revised chronostratigraphy. Quat. Sci. Rev. 28 (9), 812–829. https://doi.org/10.1016/j.quascirev.2008.12.002.

Koevoets, M.J., Hammer, Ø., Olaussen, S., Senger, K., Smelror, M., 2018. Integrating subsurface and outcrop data of the Middle Jurassic to Lower Cretaceous Agardfjellet Formation in central Spitsbergen. Norw. J. Geol. 98 (1), 1–34. https://doi.org/10.17850/njg98-4-01.

Kohl, T., Brenni, R., Eugster, W., 2002. System performance of a deep borehole heat exchanger. Geothermics 31 (6), 687–708. https://doi.org/10.1016/S0375-6505(02)00031-7.

Kristiansen, J.I., 1991. NEPR: a FORTRAN-77 program for determining thermal conductivity and diffusivity by needle-probe inversion. Comput. Geosci. 17 (3), 351–390. https://doi.org/10.1016/0098-3004(91)90046-G.

Kukkonen, I.T., Joeleht, A., 2003. Weichselian temperatures from geothermal heat flow data. J. Geophys. Res. 108, 2163. https://doi.org/10.1029/2001JB001579.

Kukkonen, I.T., Rath, V., Kivekäs, L., Šafanda, J., Čermak, V., 2011. Geothermal studies of the Outokumpu Deep Drill Hole, Finland: vertical variation in heat flow and palaeoclimatic implications. Phys. Earth Planet. Inter. 188 (1–2), 9–25. https://doi.org/10.1016/j.pepi.2011.06.002.

Kurttila, M.P.E., 2021. Borehole Thermal Energy Storage As a Seasonal Capacitor in the Off-Grid Arctic energy Supply System. NTNU, Trondheim.

Lachenbruch, A.H., Marshall, B.V., 1969. Heat flow in the Arctic. Arct. 22 (3), 300–311. https://www.jstor.org/stable/40507641.

Lasabuda, A.P., Johansen, N.S., Laberg, J.S., Faleide, J.I., Senger, K., Rydningen, T.A., Patton, H., Knutsen, S.-.M., Hanssen, A., 2021. Cenozoic uplift and erosion of the Norwegian Barents Shelf–A review. Earth Sci. Rev. 217, 103609 https://doi.org/10.1016/j.earscirev.2021.103609.

Lauritzen, S.E., Bottrell, S., 1994. Microbiological activity in thermoglacial karst springs, south Spitsbergen. Geomicrobiol. J. 12 (3), 161–173. https://doi.org/10.1080/01490459409377983.

Ledo, J., García-Merino, M., Larnier, H., Slezak, K., Piña-Varas, P., Marcuello, A., Queralt, P., Pérez, N., Schmincke, H.-.U., Sumita, M., 2021. 3D electrical resistivity of Gran Canaria island using magnetotelluric data. Geothermics 89, 101945. https://doi.org/10.1016/j.geothermics.2020.101945.

Lee, Y., Park, S., Kim, J., Kim, H.C., Koo, M.-.H., 2010. Geothermal resource assessment in Korea. Renew. Sustain. Energy Rev. 14 (8), 2392–2400. https://doi.org/10.1016/j.rser.2010.05.003.

Løseth, H., Lippard, S., Sættem, J., Fanavoll, S., Fjerdingstad, V., Leith, T., Ritter, U., Smelror, M., 1993. Cenozoic Uplift and Erosion of the Barents Sea—Evidence from the Svalis Dome area, Norwegian Petroleum Society Special Publications. Elsevier, pp. 643–664. https://doi.org/10.1016/B978-0-444-88943-0.50042-3.

Lund, J.W., Bjelm, L., Bloomquist, G., Mortensen, A.K., 2008. Characteristics, development and utilization of geothermal resources–a Nordic perspective. Episodes J. Int. Geosci. 31 (1), 140–147. https://doi.org/10.18814/epiiugs/2008/v31i1/019.

Lund, J.W., Toth, A.N., 2021. Direct utilization of geothermal energy 2020 worldwide review. Geothermics 90, 101915. https://doi.org/10.1016/j.geothermics.2020.101915.

M.D, K., G.N, A., I.M, B., E.O, K., T, K., 2015. Seismicity, heat flow and tectonics of the West-Arctic Basin. Monitor. Sci. Technol. 3 (24), 23–32.

Majorowicz, J., Grasby, S.E., 2010a. Heat flow, depth–temperature variations and stored thermal energy for enhanced geothermal systems in Canada. J. Geophys. Eng. 7 (3), 232–241. https://doi.org/10.1088/1742-2132/7/3/002.

Majorowicz, J., Grasby, S.E., 2010b. High potential regions for enhanced geothermal systems in Canada. Nat. Resour. Res. 19 (3), 177–188. https://doi.org/10.1007/s11053-010-9119-8.

Majorowicz, J., Wybraniec, S., 2011. New terrestrial heat flow map of Europe after regional paleoclimatic correction application. Int. J. Earth Sci. 100 (4), 881–887. https://doi.org/10.1007/s00531-010-0526-1.

Majorowicz, J.A., Embry, A.F., 1998. Present heat flow and paleo-geothermal regime in the Canadian Arctic margin: analysis of industrial thermal data and coalification gradients. Tectonophysics 291 (1), 141–159. https://doi.org/10.1016/S0040-1951(98)00036-5.

Marshall, C., Uguna, J., Large, D.J., Meredith, W., Jochmann, M., Friis, B., Vane, C., Spiro, B.F., Snape, C.E., Orheim, A., 2015. Geochemistry and petrology of palaeocene coals from Spitzbergen—Part 2: maturity variations and implications for local and regional burial models. Int. J. Coal Geol. 143, 1–10. https://doi.org/10.1016/j.coal.2015.03.013.

Mathiesen, A., Nielsen, L.H., Vosgerau, H., Poulsen, S.E., Bjørn, H., Røgen, B., Ditlefsen, C., Vangkilde-Pedersen, T., 2022. Geothermal energy use, country update report for Denmark. In: European Geothermal Congress 2022. Berlin, Germany, 17-22 October 2022. https://europeangeothermalcongress.eu/about-egc/.

Maystrenko, Y.P., Elvebakk, H.K., Osinska, M., Olesen, O., 2021. New heat flow data from the Veiholmen and Raudsand boreholes, middle Norway. Geothermics 89, 101964. https://doi.org/10.1016/j.geothermics.2020.101964.

McKenna, T.E., Sharp, J.M., 1998. Radiogenic Heat Production in Sendimentary Rocks of the Gulf of Mexico Basin, South Texas. Am Assoc Pet Geol Bull 82 (3), 484–496. https://doi.org/10.1306/1D9BC449-172D-11D7-8645000102C1865D.

Medvedev, S., Faleide, J.I., Hartz, E.H., 2023. Cenozoic reshaping of the Barents-Kara Shelf: influence of erosion, sedimentation, and glaciation. Geomorphology 420, 108500. https://doi.org/10.1016/j.geomorph.2022.108500.

Middleton, M.F., 1993. A transient method of measuring the thermal properties of rocks. Geophysics 58 (3), 357–365. https://doi.org/10.1190/1.1443419.

Midttømme, K., Alonso, M.J., Krafft, C.G., Kvalsvik, K.H., Ramstad, R.K., Stene, J., 2020. Geothermal energy use in Norway, country update for 2015-2019. In: Proceedings, World Geothermal Congress.

Midttømme, K., Berre, I., Hauge, A., Musæus, T.E., Kristjànsson, B.R., 2015a. Geothermal energy-country update for Norway. In: Proceedings, World Geothermal Congress.

Midttømme, K., Jochmann, M., Henne, I., Wangen, M., Thomas, P., 2015b. Is geothermal energy an alternative for Svalbard?. In: The Third Sustainable Earth Sciences Conference and Exhibition. European Association of Geoscientists & Engineers, pp. 1–5.

Midttømme, K., Roaldset, E., 1999. Thermal conductivity of sedimentary rocks: uncertainties in measurement and modelling. Geol. Society 158 (1), 45–60. https://doi.org/10.1144/GSL.SP.1999.158.01.04.

Minakov, A., 2018. Late Cenozoic lithosphere dynamics in Svalbard: interplay of glaciation, seafloor spreading and mantle convection. J. Geodyn 122, 1–16.

Mørk, M.B.E., Duncan, R.A., 1993. Late Pliocene basaltic volcanism on the Western Barents Shelf margin: implications from petrology and ^{40}Ar-^{39}Ar dating of volcaniclastic debris from a shallow drill core. Nor. Geol. Tidsskr. 73, 209–225. http://njg.geologi.no/images/NJG_articles/NGT_73_4_209-225.pdf.

Motoyama, H., Watanabe, O., Fujii, Y., Kamiyama, K., Igarashi, M., Matoba, S., Kameda, T., Goto-Azuma, K., Izumi, K., Narita, H., 2008. Analyses of ice core data from various sites in Svalbard glaciers from 1987 to 1999. NIPR Arctic data reports 7, 1–79.

Moya, D., Aldás, C., Kaparaju, P., 2018. Geothermal energy: power plant technology and direct heat applications. Renew. Sustain. Energy Rev. 94, 889–901. https://doi.org/10.1016/j.rser.2018.06.047.

Nielsen, L.H., Mathiesen, A., Bidstrup, T., 2004. Geothermal energy in Denmark. GEUS Bull. 4, 17–20. https://doi.org/10.34194/geusb.v4.4771.

Nuus, M., 2020. A Modelling-Based Approach to the Geothermal Energy Potential of Svalbard. University of Utrecht/Univesity Centre in Svalbard, Norway, p. 39.

Nyland, B., Jensen, L.N., Skagen, J., Skarpnes, O., Vorren, T., 1992. Tertiary Uplift and Erosion in the Barents Sea: magnitude, Timing and Consequences. Editors. In: Larsen, R.M., Brekke, H., Larsen, B.T., Talleraas, E. (Eds.), Structural and Tectonic Modelling and Its Application to Petroleum Geology. Elsevier, Amsterdam, pp. 153–162. https://doi.org/10.1016/B978-0-444-88607-1.50015-2.

Ohm, S.E., Larsen, L., Olaussen, S., Senger, K., Birchall, T., Demchuk, T., Hodson, A., Johansen, I., Titlestad, G.O., Karlsen, D.A., 2019. Discovery of shale gas in organic-rich Jurassic successions, Adventdalen, Central Spitsbergen, Norway. Nor. Geol. Tidsskr. 99 (2), 349–376. https://doi.org/10.17850/njg007.

Olaussen, S. and Birchall, T., 2022. Rapport om berggrunnsgeologi og brønnprognose.

Olaussen, S., Grundvåg, S.-A., Senger, K., Anell, I., Betlem, P., Birchall, T., Braathen, A., Dallmann, W., Jochmann, M., Johannessen, E.P., Lord, G., Mørk, A., Osmundsen, P. T., Smyrak-Sikora, A., Stemmerik, L., 2023. The Svalbard carboniferous to cenozoic composite tectono-stratigraphic element. Geolog. Society, London, Memoirs 57 (1). https://doi.org/10.1144/M57-2021-36. M57-2021-36.

Olaussen, S., Senger, K., Braathen, A., Grundvåg, S.A., Mørk, A., 2019. You learn as long as you drill; research synthesis from the Longyearbyen CO2 Laboratory, Svalbard, Norway. Norw. J. Geol. 99, 157–187. https://doi.org/10.17850/njg008.

Olichwer, T., Tarka, R., 2018. Thermal and mineral springs of southern Spitsbergen. Polish Polar Res. 39 (3).

Pascal, C., 2015. Heat flow of Norway and its continental shelf. Mar. Pet. Geol. 66, 956–969. https://doi.org/10.1016/j.marpetgeo.2015.08.006.

Pascal, C., 2022. 3D thermal modelling of the Oslo-Asker area, Norway. Geothermics 103, 102430. https://doi.org/10.1016/j.geothermics.2022.102430.

Pascal, C., Balling, N., Barrère, C., Davidsen, B., Ebbing, J., Elvebakk, H., Mesli, M., Roberts, D., Slagstad, T. and Willemoes-Wissing, B., 2010a. HeatBar Final Report 2010, Basement Heat Generation and Heat Flow in the western Barents Sea - Importance for hydrocarbon systems.

Pascal, C., Elvebakk, H., Olesen, O., 2010b. An assessment of deep geothermal resources in Norway. In: Abstracts and Proceedings, World Geothermal Congress. Bali, Indonesia, 25–29 April.

Peng, C., Pan, B., Xue, L., Liu, H., 2019. Geophysical survey of geothermal energy potential in the Liaoji Belt, northeastern China. Geoth. Energy 7 (1), 14. https://doi.org/10.1186/s40517-019-0130-y.

Popov, Y.A., Pevzner, S.L., Pimenov, V.P., Romushkevich, R.A., 1999a. New geothermal data from the Kola superdeep well SG-3. Tectonophysics 345–366.

Popov, Y.A., Pribnow, D.F.C., Sass, J.H., Williams, C.F., Burkhardt, H., 1999b. Characterization of rock thermal conductivity by high-resolution optical scanning. Geothermics 28 (2), 253–276. https://doi.org/10.1016/S0375-6505(99)00007-3.

Prestvik, T., 1978. Cenozoic plateau lavas of Spitsbergen - a geochemical study. Aarb., Nor. Polarinst. 1977, 129–143. https://core.ac.uk/download/pdf/30874199.pdf#page=131.

Reigstad, L.J., Jorgensen, S.L., Lauritzen, S.-.E., Schleper, C., Urich, T., 2011. Sulfur-oxidizing chemolithotrophic proteobacteria dominate the microbiota in high arctic thermal springs on Svalbard. Astrobiology 11 (7), 665–678. https://doi.org/10.1089/ast.2010.0551.

Richter, A., 2021. Geothermal could replace coal on arctic island group of Svalbard. Think Geoenergy. https://www.thinkgeoenergy.com/geothermal-could-replace-coal-on-arctic-island-group-of-svalbard/.

Ringkjøb, H.-.K., Haugan, P.M., Nybø, A., 2020. Transitioning remote Arctic settlements to renewable energy systems–A modelling study of Longyearbyen. Svalbard. Appl. Energy 258, 114079. https://doi.org/10.1016/j.apenergy.2019.114079.

Sættem, J., 1988. Varmestrømsmålinger i Barentshavet. 18. Nordiske Geologiske Vintermøde, Geological Survey of Denmark 406–408.

Salvigsen, O., Elgersma, A., 1985. Large-scale karst features and open taliks at Vardeborgsletta, outer Isfjorden, Svalbard. Polar Res 3 (2), 145–153. https://doi.org/10.3402/polar.v3i2.6948.

Schäfer, M., Gillet-Chaulet, F., Gladstone, R., Pettersson, R., A Pohjola, V., Strozzi, T., Zwinger, T., 2014. Assessment of heat sources on the control of fast flow of Vestfonna ice cap, Svalbard. The Cryosphere 8 (5), 1951–1973. https://doi.org/10.5194/tc-8-1951-2014.

Schintgen, T., 2015. Exploration for deep geothermal reservoirs in Luxembourg and the surroundings-perspectives of geothermal energy use. Geoth. Energy 3 (1), 1–30. https://doi.org/10.1186/s40517-015-0028-2.

Selway, K., Smirnov, M.Y., Beka, T., O'Donnell, J.P., Minakov, A., Senger, K., Faleide, J. I., Kalscheuer, T., 2020. Magnetotelluric Constraints on the Temperature, Composition, Partial Melt Content, and Viscosity of the Upper Mantle Beneath Svalbard. Geochem. Geophys. Geosyst. 21 (5) https://doi.org/10.1029/2020GC008985 e2020GC008985.

Senger, K., Brugmans, P., Grundvåg, S.-.A., Jochmann, M., Nøttvedt, A., Olaussen, S., Skotte, A., Smyrak-Sikora, A., 2019. Petroleum exploration and research drilling onshore Svalbard: a historical perspective. Norw. J. Geol. 99 (3), 1–30. https://doi.org/10.17850/njg99-3-1.

Senger, K. and Galland, O., 2022. Stratigraphic and Spatial extent of HALIP Magmatism in central Spitsbergen Geochemistry Geophysics Geosystems.

Senger, K., Smyrak-Sikora, A., Kuckero, L., Rodes, N. and Betlem, P., 2022. Svalbard Rock Vault - liberating vintage geoscience data from Svalbard (0.0.1) https://doi.org/10.5281/zenodo.5919082.

Senger, K., Tveranger, J., Ogata, K., Braathen, A., Planke, S., 2014. Late Mesozoic magmatism in Svalbard: a review. Earth Sci. Rev. 139, 123–144.

Simmons, G., 1961. Anisotropic thermal conductivity. J Geophys. Res. 66 (7), 2269–2270. https://doi.org/10.1029/JZ066i007p02269.

Skjelkvåle, B.-.L., Amundsen, H.E.F., O'Reilly, S.Y., Griffin, W.L., Gjelsvik, T., 1989. A primitive alkali basaltic stratovolcano and associated eruptive centres, Northwestern Spitsbergen: volcanology and tectonic significance. J. Volcanol. Geotherm. Res. 37 (1), 1–19. https://doi.org/10.1016/0377-0273(89)90110-8.

Slagstad, T., Balling, N., Elvebakk, H., Midttømme, K., Olesen, O., Olsen, L., Pascal, C., 2009. Heat-flow measurements in Late Palaeoproterozoic to Permian geological provinces in south and central Norway and a new heat-flow map of Fennoscandia and the Norwegian–Greenland Sea. Tectonophysics 473 (3), 341–361. https://doi.org/10.1016/j.tecto.2009.03.007.

Smith, D.P., 2019. Fitting geothermal energy into the energy transition. Neth. J. Geosci. 98. https://doi.org/10.1017/njg.2019.5.

Smyrak-Sikora, A., Johannessen, E.P., Olaussen, S., Sandal, G., Braathen, A., 2019. Sedimentary architecture during Carboniferous rift initiation–the arid Billefjorden Trough, Svalbard. J. Geol. Soc. London 176 (2), 225–252. https://doi.org/10.1144/jgs2018-100.

Smyrak-Sikora, A., Nicolaisen, J., Braathen, A., Johannessen, E.P., Olaussen, S., Stemmerik, L., 2021. Impact of growth faults on mixed siliciclastic-carbonate-evaporite deposits during rift climax and reorganisation—Billefjorden Trough, Svalbard, Norway. Basin Res. 1–32. https://doi.org/10.1111/bre.12578.

Smyrak-Sikora, A., Augland, L.E., Betlem, P., Grundvåg, S.-A., Helland-Hansen, W., Jelby, M.E., Jensen, M.A., Jochmann, M.M., Johanessen, E.P., Jones, M.T., Koevoets-Westerduin, M., Lord, G.S., Mørk, A., Olaussen, S., Planke, S., Senger, K., Stemmerik, L., Vickers, M., Śliwińska, K.K., Zuchuat, V., 2022. Deep-time paleoclimate archive in High Arctic, Svalbard, Norway, EGU General Assembly, Vienna, Austria, 23-27 May, https://doi.org/10.5194/egusphere-egu22-7172.

Snoen, K.B., 2021. Pre-investigations For High Temperature Borehole Thermal Energy Storage: A part of the Future Energy Solution in Longyearbyen, Svalbard? NTNU, Trondheim.

SNSK, 2022. Utvikling av termisk energiforsyning på Svalbard basert på dype energibrønner. Enova konseptutredning, prosjektnummer 21–957.

Solheim, A., Faleide, J.I., Andersen, E.S., ElverhØI, A., Forsberg, C.F., Vanneste, K., Uenzelmann-Neben, G., Channell, J.E.T., 1998. Late Cenozoic seismic stratigraphy

and glacial geological development of the East Greenland and Svalbard-Barents Sea continental margins. Quat. Sci. Rev. 17 (1), 155–184. https://doi.org/10.1016/S0277-3791(97)00068-1.

Sommer, W., Valstar, J., Leusbrock, I., Grotenhuis, T., Rijnaarts, H., 2015. Optimization and spatial pattern of large-scale aquifer thermal energy storage. Appl. Energy 137, 322–337. https://doi.org/10.1016/j.apenergy.2014.10.019.

Somogyi, V., Sebestyén, V., Nagy, G., 2017. Scientific achievements and regulation of shallow geothermal systems in six European countries – a review. Renew. Sustain. Energy Rev. 68, 934–952. https://doi.org/10.1016/j.rser.2016.02.014.

Stemmerik, L., 2008. Influence of late Paleozoic Gondwana glaciations on the depositional evolution of the northern Pangean shelf, North Greenland, Svalbard, and the Barents Sea. Editors. In: Fielding, C.R., Frank, T.D., Isbell, J.L. (Eds.), Resolving the Late Paleozoic ice Age in Time and Space. Geological Society of America, pp. 205–217. https://doi.org/10.1130/SPE441.

Sundvor, E., 1986. Heat Flow Measurements On the Western Svalbard Margin. University of Bergen, Seismological Observatory. Int. Rep.

Sundvor, E., Austegard, A., 1990. The Evolution of the Svalbard margins: Synthesis and New results, Geological History of the Polar Oceans: Arctic Versus Antarctic. Springer, pp. 77–94.

Sundvor, E., Eldholm, O., Gladczenko, T.P., Planke, S., 2000. Norwegian-Greenland sea thermal field. Geological Society 167 (1), 397–410. https://doi.org/10.1144/GSL.SP.2000.167.01.15.

Sundvor, E., Myhre, A.M., Eldholm, O., 1989. Heat Flow Measurements On the Norwegian continental Margin During the FLUNORGE project. Seismological Observatory. University of Bergen.

Swanberg, C.A., Morgan, P., Boulos, F., 1983. Geothermal potential of Egypt. Tectonophysics 96 (1–2), 77–94. https://doi.org/10.1016/0040-1951(83)90245-7.

Vagnes, E., Amundsen, H.E.F., 1993. Late Cenozoic uplift and volcanism on Spitsbergen: caused by mantle convection? Geology 21 (3), 251–254. https://doi.org/10.1130/0091-7613(1993)021<0251:LCUAVO>2.3.CO;2.

van de Wal, R.S.W., Mulvaney, R., Isaksson, E., Moore, J.C., Pinglot, J.F., Pohjola, V.A., Thomassen, M.P.A., 2002. Reconstruction of the historical temperature trend from measurements in a medium-length borehole on the Lomonosovfonna plateau, Svalbard. Ann. Glaciol. 35, 371–378. https://doi.org/10.3189/172756402781816979.

Vanneste, M., Guidard, S., Mienert, J., 2005. Bottom-simulating reflections and geothermal gradients across the western Svalbard margin. Terra Nova 17 (6), 510–516. https://doi.org/10.1111/j.1365-3121.2005.00643.x.

Vogt, P.R., Sundvor, E., 1996. Heat flow highs on the Norwegian-Barents-Svalbard continental slope: deep crustal fractures, dewatering, or “memory in the mud”? Geophys Res Lett 23 (24), 3571–3574. https://doi.org/10.1029/96GL03259.

Von Herzen, R., Maxwell, A., 1959. The measurement of thermal conductivity of deep-sea sediments by a needle-probe method. J Geophys Res 64 (10), 1557–1563. https://doi.org/10.1029/JZ064i010p01557.

Ylvisåker, L.N., 2021. Drilling For Heat Storage in Svalbard. High North News. https://www.highnorthnews.com/en/drilling-heat-storage-svalbard.

Zagorodnov, V., Sinkevich, S., Arkhipov, S., 1989. Ice core express-analysis for structure and thermal regime studies of Austfonna. Data Glaciol. Stud. 66, 149–158.

Zielinski, G., Gunleiksrud, T., Sættem, J., Zuidberg, H., Geise, J., 1986. Deep heatflow measurements in quaternary sediments on the Norwegian continental shelf. In: Offshore Technology Conference. OnePetro.

Zuchuat, V., Sleveland, A., Twitchett, R., Svensen, H., Turner, H., Augland, L., Jones, M., Hammer, Ø., Hauksson, B., Haflidason, H., 2020. A new high-resolution stratigraphic and palaeoenvironmental record spanning the End-Permian Mass Extinction and its aftermath in central Spitsbergen, Svalbard. Palaeogeogr Palaeoclimatol Palaeoecol, 109732.